RNA binding proteins ZFP36L1 and ZFP36L2 promote cell quiescence

[1]Alison Galloway, [1]Alexander Saveliev, [1,7]Sebastian Łukasiak, [1,5]Daniel J. Hodson, [2]Daniel Bolland, [3]Kathryn Balmanno, [1]Helena Ahlfors, [1,6]Elisa Monzón-Casanova, [1,8]Sara Ciullini Mannurita, [1]Lewis S. Bell, [4]Simon Andrews, [1]Manuel D. Díaz-Muñoz, [3]Simon J. Cook, [2]Anne Corcoran, and [1]Martin Turner*.

[1]Laboratory of Lymphocyte Signalling and Development, [2]Laboratory of Nuclear Dynamics, [3]Laboratory of Signalling, [4]Bioinformatics Group, The Babraham Institute, Cambridge CB22 3AT, UK. [5]Department of Haematology, University of Cambridge, The Clifford Allbutt Building, Cambridge Biomedical Campus, Hills Road, Cambridge CB2 0AH, UK. [6]Department of Biochemistry, University of Cambridge, Tennis Court Road, Cambridge CB2 1QW, UK.

*Correspondence to: martin.turner@babraham.ac.uk

Abstract

Progression through the stages of lymphocyte development requires coordination of the cell cycle. Such coordination ensures genomic integrity while cells somatically rearrange their antigen receptors (in a process called VDJ recombination) and upon successful rearrangement, expands their pools of progenitor lymphocytes. Here, we show that in developing B lymphocytes the RNA binding proteins (RBPs) ZFP36L1 and ZFP36L2 are critical for maintaining quiescence prior to pre-B cell receptor (BCR) expression and for re-establishing quiescence following pre-BCR-induced expansion. These RBPs suppress an evolutionarily conserved post-transcriptional regulon consisting of mRNAs whose protein products cooperatively promote transition into the S phase of the cell cycle. This mechanism promotes VDJ recombination and effective selection of Igμ$^+$ cells at the pre-BCR checkpoint.

One sentence summary: The RNA binding proteins ZFP36L1 and ZFP36L2 enforce quiescence on developing lymphocytes by suppressing mRNAs that promote cell cycle progression.

Lymphocyte development is characterized by dynamic shifts between quiescence and proliferation. Quiescence promotes VDJ recombination, the process that generates immunoglobulin and T cell receptor genes, since RAG2 protein expression is restricted to the G_0/G_1 phase of the cell cycle (*1-3*). In B cells VDJ recombination leads to expression of an immunoglobulin-μ (Igμ) heavy chain that, together with the surrogate light chains, forms a pre-B cell receptor (pre-BCR). Signals from the pre-BCR terminate the recombination process and trigger rapid proliferation associated with passage through the pre-BCR checkpoint (*4*). Later signals from the pre-BCR re-establish quiescence allowing immunoglobulin light chain recombination (*5, 6*) (fig. S1A).

The ZFP36 family of RNA binding proteins (RBPs) regulate gene expression post-transcriptionally by promoting mRNA decay (*7*). This requires their direct binding to AU-rich elements (AREs) located in the 3' untranslated regions (UTRs) of mRNAs. ZFP36 destabilizes cytokine mRNAs and exerts an anti-inflammatory function (*8, 9*). In addition, ZFP36 antagonizes *Myc*-induced lymphomagenesis (*10*), and its paralogs ZFP36L1 and ZFP36L2 have redundant roles in preventing T cell leukemia in mice (*11*) however, the pathways controlled by these RBPs remain poorly understood.

All three ZFP36 family mRNAs were expressed throughout B cell development (fig. S1B). Conditional genetic deletion demonstrated redundant roles for ZFP36L1 and ZFP36L2 in early B cell development that cannot be compensated for by endogenous ZFP36 and were independent of NOTCH1, a known target of these RBP (fig. S2) (*11*), thus we generated mice where *Zfp36l1* and *Zfp36l2* are deleted in pro-B cells (fig. S3). For simplicity $Zfp36l1^{fl/fl}$ $Zfp36l2^{fl/fl}$ $Mb1^{cre/+}$ mice will be referred to as DCKOs (double conditional knockout) and their $Zfp36l1^{fl/fl}$ $Zfp36l2^{fl/fl}$ $Mb1^{+/+}$ littermates as controls. DCKO mice displayed reduced cellularity from the pre-B stage onwards culminating in a 98% reduction in mature-B cell number (**Fig. 1A, B**). The proportion of $CD43^+$ cells expressing Igμ was greatly diminished (**Fig. 1C**), and a variable proportion of DCKO cells transited the pre-BCR checkpoint without Igμ expression (**Fig. 1D**). Within the compartment enriched for pro-B cells, DCKOs had reduced proportions of cells containing one or two V to DJ recombined IgH alleles (**Fig. 1E,** fig. S4). At later developmental stages the DCKOs failed to increase the proportion of recombined IgH alleles to control levels. Notably the decrease in the proportion of V to DJ recombined IgH alleles and $Igμ^+$ cells within the pro/early pre-B cell compartment of DCKOs is similar suggesting that the failure to express Igμ is not due to an increase in non-productive joints. Similarly, V-J recombination of the Igκ light chain locus was reduced in DCKO late pre-B cells (**Fig. 1F**).

Thus DCKO mice display reduced B cell numbers, delayed VDJ recombination and failure of the pre-BCR checkpoint.

Expression of a productively rearranged Igμ-transgene failed to restore late pre-, immature-, or mature-B cell numbers in DCKO mice indicating that reduced VDJ recombination of IgH is not the sole defect (fig. S5). Consistent with this we observed an increase in apoptosis of DCKO $Igμ^+$ late pre-B cells (**Fig. 1G)**. The increased apoptosis was not susceptible to inhibition by BCL2, and we did not detect a DNA damage response (fig. S6). Notably, in both DCKOs and controls a substantial number of $Igμ^-$ cells in the late pre-B cell gate were apoptotic indicating that although $Igμ^-$ DCKO cells were aberrantly selected, they did not bypass the requirement of pre-BCR expression for continued survival (**Fig. 1H**).

Within mRNAs overrepresented in DCKO late pre-B cell transcriptomes there was a strong enrichment for pathways promoting cell cycle progression (**Fig. 2A, B, tables S1-4**). Since VDJ recombination is inhibited by cell cycle progression, and the pre-BCR checkpoint is mediated by the selective proliferation of $Igμ^+$ cells, we hypothesized that these aspects of the phenotype might be explained by uncontrolled cell cycle progression in DCKOs. The apoptosis of DCKO late pre-B cells could be due to delayed light chain recombination or overexpression of cell cycle regulators; these cells are destined to be quiescent and therefore may not tolerate activation of the E2F pathway, which regulates transition through the cell cycle and DNA synthesis. Indeed, loss of *E2f1* has been demonstrated to increase late pre-B cell numbers (*12*).

Cell cycle analysis showed an increase in the proportion of DCKO pro-B cells in S-phase (**Fig. 2C, D**). The cyclin dependent kinase inhibitor p27 (CDKN1B) is known to regulate the cell cycle during pre-B cell development (*5*) and high expression of p27 is a marker of cellular quiescence (*13*). The proportion of $p27^{high}$ G_0 cells was markedly reduced in DCKO pro-B cells, and was moderately reduced in DCKO early and late pre-B cells (**Fig. 2E, F**). Thus ZFP36L1 and ZFP36L2 impose quiescence on developing B cells and inhibit S-phase entry prior to expression of the pre-BCR.

We demonstrated the transcription factors induced by the pre-BCR that promote quiescence in late pre-B cells were expressed in DCKOs and p27 mRNA induced; additionally factors mediating VDJ recombination were expressed and the Igκ locus was transcriptionally active (fig. S7). Therefore DCKO late pre-B cells are transcriptionally poised to enter quiescence and

undergo VDJ recombination, but post-transcriptional regulation mediated by ZFP36L1 and ZFP36L2 is required for the full activation of these processes.

Consistent with their role in promoting mRNA decay, ZFP36L1-bound transcripts identified by crosslinking immunoprecipitation (iCLIP) (*14*) were found to be increased in abundance in DCKO late pre-B cells (**Fig. 3A**). Increased mRNA abundance in DCKO late pre-B cells was also associated with AREs in the 3'UTRs of mRNAs (fig. S8A), and with Zfp36 binding sites in the human homologs of mouse transcripts (*15*) (fig. S8B, C). Thus, the specificity of ZFP36 family proteins is generally conserved across family members, species and cell types.

ZFP36L1 binding sites were typically associated with AREs (table S5). Amongst mRNAs identified in the iCLIP, cell cycle pathways were strongly enriched (tables S6 and S7) further connecting ZFP36L1 to cell cycle regulation. Within mRNAs implicated in cell cycle control we identified several candidate targets that have ZFP36L1 binding sites, or AREs, and significant increases in mRNA abundance in DCKO late pre-B cells (**Fig. 3B**, table S8). We validated the activity of the ZFP36L1 binding site in *Ccne2* (fig. S9). Notably, among the putative targets are the mRNAs encoding PIM family kinases and components of the CDK2-CyclinE complex that phosphorylates p27, promoting its destruction (*16, 17*); this mechanism is consistent with the reduced p27 protein, but equivalent p27 mRNA in DCKO late pre-B cells. Furthermore, the AREs in putative target mRNAs with roles in cell cycle progression were very highly conserved within mammals (**Fig. 3C**). These data strongly suggest that ZFP36L1 and ZFP36L2 directly regulate an evolutionarily-conserved post-transcriptional regulon controlling cell cycle progression (*18*).

A post-transcriptional mechanism for enforcing quiescence is well suited to the events surrounding the pre-BCR checkpoint because it can be reversed more rapidly than changes mediated at the level of transcription. ZFP36L1 and ZFP36L2 are phosphorylated by MAPKAP2 downstream of p38 MAPK and this inhibits their mRNA destabilizing effects (*19*). Importantly, p38 activity is induced downstream of the pre-BCR providing a mechanism to relieve the repression of mRNAs encoding cell cycle regulators by ZFP36L1 and ZFP36L2 (*20*). To examine the effects of ZFP36L1 overexpression at the pre-BCR checkpoint we generated mice that conditionally express ZFP36L1 fused at its N-terminus to green fluorescent protein (GFP); we refer to the allele as $ROSA26^{L1}$ (fig. S10). There was a significantly reduced proportion of S phase cells and increased proportion of G_0 cells in $ROSA26^{L1/L1}$ *CD2cre* pre-B

cells compared to controls (**Fig. 3D, E,** fig. S11A, B). Thus enforced expression of ZFP36L1 suppresses proliferation at the pre-BCR checkpoint.

CyclinD3, CyclinE2 and their partner kinases were identified amongst candidate ZFP36L1/2 targets in DCKO late pre-B cells. CyclinD3 has an essential role in pre-BCR mediated proliferation (*21*). Elevated protein expression of CyclinD3 and CyclinE2 was confirmed in DCKO pro- and early pre-B cells (**Fig. 4A, B**, fig. S12A, B) indicating that ZFP36L1 and ZFP36L2 limit the induction of CyclinD3 and CyclinE2 to those cells that are transiting pre-BCR selection. By contrast, *ROSA26*^{L1} *CD2cre* mice failed to properly induce CyclinD3 or CyclinE2 at the proliferative early pre-B cell stage, further reinforcing the role of ZFP36L1 in the control of cell cycle at the point of pre-BCR selection (**Fig. 4C, D**, fig. S12C- E).

Overexpression of CyclinD3 can inhibit VDJ recombination in pre-B cells through a mechanism involving loss of quiescence (*22*). Therefore we treated DCKO and control mice with the CDK4/6 inhibitor palbociclib, which inhibits activation of the E2F pathway. Palbociclib treatment increased V-DJ recombination at the IgH locus of pro/early pre-B cells (**Fig. 4E,** fig. S13A, B). Consistent with increased recombination and reduced cell division, the proportion of pro- and pre-B cells containing excised signal circles was increased following palbociclib treatment (fig. S13C, D). Conversely the frequency of recombination at the IgH locus of late pre-B cells was not rescued by palbociclib treatment reflecting the inhibition of the cell cycle which prevents the proliferative selection of cells into the late pre-B cell pool (fig. S13E). Igκ recombination was also restored in DCKO late pre-B cells following palbociclib treatment (**Fig. 4F,** fig. S13F). This indicates that the delays in VDJ recombination are caused by loss of quiescence in DCKO pro- and pre-B cells.

We found that increased *Zfp36* family member mRNA expression was typically associated with quiescent cell phenotypes (**Fig. 4G**). Therefore, we generated a *ZFP36L1*$^{-/-}$ HCT116 human colorectal carcinoma cell line and measured expression of CyclinD3 and of CyclinD1- a putative ZFP36L1 target that is not expressed in B cells (*15*, *23*). Expression of both D-type cyclins was increased in *ZFP36L1*$^{-/-}$ HCT116 cells compared to the parental line (**Fig. 4H**). Additionally, genetic experiments have shown loss of *Zfp36l2* leads to depletion of hematopoietic stem cells (*24*), loss of *Zfp36* is associated with increased muscle satellite activation (*25*). Thus these RBPs likely form part of a general mechanism for the post-transcriptional regulation of quiescence.

As many as 10% of human mRNAs contain AREs (*26*); this may enable interdependent cellular processes to be coordinated by the ZFP36 family. The dynamics of the G_0/G_1-S phase transition are characterized by switching behavior mediated by positive feed-forward regulation in the E2F pathway (*27*), thus this pathway may be particularly sensitive to moderate changes in the abundance of its components as measured in DCKO pre-B cells (**Fig. 3A**). We propose that ZFP36L1 and ZFP36L2 suppress the expression of limiting factors for E2F pathway activation (*16, 28-31*) and DNA replication licensing thus providing a robust mechanism for reversibly stabilizing the G_0/G_1 state. This mechanism would contribute to the ability of the progenitor cell populations to respond appropriately and dynamically to both mitogenic and anti-proliferative signals.

Supplementary Materials

Materials and Methods

Figs. S1 to S13

Tables S1 to S16

References (32–50)

Figure legends

Figure 1: Conditional knockout of *Zfp36l1* and *Zfp36l1* in pro-B cells abrogates pre-B cell development. (A) Representative scatter plots from flow cytometric analysis of B cell development in control and DCKO bone marrow. Numbers on plots indicate percentage of plotted cells in the gate. (B) Quantification of B cell developmental subsets in control (n=5) and DCKO (n=5) bone marrow from flow cytometry data shown in (A). Control and DCKO populations were compared by an ANOVA with Sidak's post-test. Symbols indicate biological replicates, bars represent geometric means. Data are representative of two independent experiments. (C, D) Flow cytometry measuring intracellular Igμ in control (n=6) and DCKO (n=5) pro- and early pre-B cells (C), and control (n=7) and DCKO (n=7) late pre-B cells (D). Representative histograms of flow cytometry data and summary data are shown. Symbols on charts indicate biological replicates, bars represent means. Control and DCKO populations were compared with a Student's t-test. Data are representative of four (C) or two (D) independent experiments. (E) Quantification of cells with zero, one, or two V to DJ recombined IgH alleles by DNA FISH within the $CD24^{low}$ pro/early pre-B (enriched for pro-B cells, n=3 biological replicates), $CD24^{high}$ pro/early pre-B (enriched for early pre-B cells, n=1 biological replicate) or late pre-B (n=3 biological replicates) populations of control and DCKO mice. Data are from a single experiment, bars represent mean values, error bars indicate the standard deviation. (F) Abundance of recombined Igκ alleles in the late pre-B cells of control (n=11) and DCKO (n=11) mice measured by qPCR. Control and DCKO samples were compared using the Student's t-test. Data are included from three independent experiments. (G, H) Proportion of control (n=5) and DCKO (n=5) pro- and pre-B cells (G), or the $Igμ^{-}$ cells appearing in the late pre-B cell gate (H), in early apoptosis measured by staining for activated caspases using FITC-VAD-FMK. Control and DCKO samples were compared by an ANOVA with Sidak's post-test, symbols indicate biological replicates, and bars represent means. Data are representative of two independent experiments.

Figure 2: *Zfp36l1* and *Zfp36l2* control the cell cycle during B cell development. (A) Gene set enrichment analysis of transcripts significantly increased in DCKO late pre-B cells. The 20 pathways with the lowest false discovery rates (FDR) calculated using the Benjamini-Hochberg correction are shown. FDR $<10^{\wedge-6}$ for all gene sets shown. Numbers beside bars represent the number of overlapping genes between the gene set and the list of transcripts increased in DCKO late pre-B cells. Dataset abbreviations are as follows: REAC (Reactome), BIOC (Biocarta), WIKI (Wikipathways), and KEGG (Kegg pathways). (B) Scatter plot showing the average reads per kilobase per million (RPKM) in DCKO and control late pre-B cells for all genes (grey) and genes in the Reactome Cell Cycle pathway gene set which are either significantly increased in the DCKO (red), unchanged (black) or significantly decreased in the DCKO (blue). (C) Representative scatter plots from intracellular flow cytometry measuring BrdU incorporation following 2.5 hours labelling *in vivo* in control and DCKO pro and pre-B cells. (D) Proportion of control (n=5) and DCKO (n=5) pro and pre-B cells incorporating BrdU measured by flow cytometry as shown in (C). Data are representative of two independent experiments. (E) Representative scatter plots from intracellular flow cytometry measuring p27 in control and DCKO pro- and pre-B cells. (F) Proportion of control (n=6) and DCKO (n=5) pro and pre-B cells in G_0 (expressing p27) measured by flow cytometry as shown in (E). Data are representative of two independent experiments. Numbers on flow cytometry dot plots indicate the percent of plotted cells in the gate. Flow cytometry data for control and DCKO samples were compared by an ANOVA with Sidak's post-test, symbols indicate biological replicates, and bars represent means.

Figure 3: Cell cycle mRNAs are direct targets of ZFP36L1 and ZFP36L2. The abundance of mRNAs in DCKO and control late pre-B cells was measured by RNA sequencing and was analyzed in DESeq. ZFP36L1 target mRNAs were identified by iCLIP in mitogen stimulated lymph node B cells. (A) The moderated log2 fold change in abundance of RNA in DCKO compared to control late pre-B cells grouped according to the number of ZFP36L1 iCLIP reads within significant peaks (FDR<5%) in the 3'UTR of each gene. n indicates the number of genes in each group. Boxes show median and interquartile range, whiskers indicate the 5^{th} and 95^{th} percentiles. Groups of mRNAs were compared by ANOVA with Tukey's post-test.
(B) Venn diagram of cell cycle mRNAs showing the overlap between mRNAs identified as ZFP36L1 targets through iCLIP, mRNAs with WWAUUUAWW motifs in their 3'UTRs, and mRNAs significantly increased in the DCKO late pre-B cells compared to control late pre-B cells as determined by a negative binomial test with a Benjamini-Hochberg correction for multiple testing in DESeq. The moderated log2 fold changes in mRNA abundance in DCKO late pre-B cells for selected groups of mRNAs are shown. (C) Sequence conservation between *H. sapiens, M. musculus, L. Africana, P. vampyrus, C. lupus familaris* and *B. Taurus* CDS, 3'UTRs and WWAUUUAWW motifs for selected mRNAs encoding cell cycle regulators. (D) Proportion of pro- and pre-B cells from *ROSA26*$^{L1/L1}$ (n=7) and *ROSA26*$^{L1/L1}$ *CD2cre* (n=10) mice incorporating BrdU, determined by flow cytometry following 2.5 hours labelling *in vivo*. Flow cytometry scatter plots shown in fig. S11A. Data are combined from two independent experiments. (D) Proportion of cells expressing p27 in *ROSA26*$^{L1/L1}$ (n=7) and *ROSA26*$^{L1/L1}$ *CD2cre* (n=6) pro- and pre-B cells. Flow cytometry scatter plots are shown in fig. S11B. Data are from a single experiment. Flow cytometry data for control and DCKO samples were compared by an ANOVA with Sidak's post-test, symbols indicate biological replicates, and bars represent means.

Figure 4: Cyclin expression is repressed by ZFP36L1 and ZFP36L2 in B cell development and this mechanism is required for efficient light chain recombination. (A) MFI (median fluorescence intensity) of flow cytometry stains for CyclinD3 in control (n=4) and DCKO (n=5) pro- and pre-B cells. Scatter plots of flow cytometry are shown in fig. S12A. Data are representative of two independent experiments. (B) MFI of flow cytometry stains for CyclinE2 in control (n=5) and DCKO (n=4) pro- and pre-B cells. Scatter plots of flow cytometry are shown in fig. S12B. Data are representative of two independent experiments. (C) MFI of flow cytometry stains for CyclinD3 in *ROSA26*$^{L1/L1}$ control (n=5) and *Cd2cre* (n=5) pro- and pre-B cells. Scatter plots of flow cytometry are shown in fig. S12C. Data are from a single experiment. (D) MFI of flow cytometry stains for CyclinE2 in *ROSA26*$^{L1/L1}$ control (n=5) and *Cd2cre* (n=5) pro- and pre-B cells. Scatter plots of flow cytometry are shown in fig. S12D. Data are from a single experiment. Flow cytometry data (A-D) were compared using an ANOVA with Tukey's post-test, symbols indicate biological replicates, and bars represent means. (E) Quantification of pro/early pre-B cells with zero, one, or two V to DJ recombined IgH alleles by DNA FISH in control and DCKO mice following treatment with vehicle control or 150mg/kg palbociclib daily for two days. Data are from a single experiment, n=3 for each group, bars represent mean values, error bars indicate the standard deviation. (F) Abundance of recombined Igκ alleles, measured by qPCR, in the late pre-B cells of control and DCKO mice treated with vehicle control or 150mg/kg palbociclib daily for two days. Control and DCKO samples were compared using an ANOVA with Tukey's post test. Data are from a single experiment, symbols represent biological replicates, bars indicate means. (G) The fold change in expression of *Zfp36* family members in published datasets comparing resting (quiescent) and stimulated dividing (non-quiescent) follicular B cells, light zone (quiescent) and dark zone (non-quiescent) germinal center-B cells (n=2), naïve (quiescent) and effector (non-quiescent) CD8^{+} T cells, adult (quiescent) and fetal (non-quiescent) hematopoietic stem cells (HSCs) (n=2), p27^{high} (quiescent) and p27^{low} (non-quiescent) fibroblasts (n=4), and resting (quiescent) and activated (non-quiescent) muscle satellite cells (n=3). * indicates a p value less than 0.05. Solid lines separate independent datasets, dashed lines separate biological replicates. (H) Expression of ZFP36L1, CyclinD3 and CyclinD1 proteins in parental and *ZFP36L1*$^{-/-}$ HCT116 colon carcinoma cells following serum starvation and restimulation; C= continuous culture, SF= serum free for 24 hours. Data are representative of three experiments.

References

1. K. Johnson *et al.*, IL-7 functionally segregates the pro-B cell stage by regulating transcription of recombination mediators across cell cycle. *J Immunol* **188**, 6084 (Jun 15, 2012).
2. S. C. Bendall *et al.*, Single-cell trajectory detection uncovers progression and regulatory coordination in human B cell development. *Cell* **157**, 714 (Apr 24, 2014).
3. L. Zhang, T. L. Reynolds, X. Shan, S. Desiderio, Coupling of V(D)J recombination to the cell cycle suppresses genomic instability and lymphoid tumorigenesis. *Immunity* **34**, 163 (Feb 25, 2011).
4. I. L. Martensson, N. Almqvist, O. Grimsholm, A. I. Bernardi, The pre-B cell receptor checkpoint. *FEBS letters* **584**, 2572 (Jun 18, 2010).
5. S. Ma *et al.*, Ikaros and Aiolos inhibit pre-B-cell proliferation by directly suppressing c-Myc expression. *Mol Cell Biol* **30**, 4149 (Sep, 2010).
6. M. R. Clark, M. Mandal, K. Ochiai, H. Singh, Orchestrating B cell lymphopoiesis through interplay of IL-7 receptor and pre-B cell receptor signalling. *Nature reviews. Immunology* **14**, 69 (Feb, 2014).
7. S. A. Brooks, P. J. Blackshear, Tristetraprolin (TTP): interactions with mRNA and proteins, and current thoughts on mechanisms of action. *Biochim Biophys Acta* **1829**, 666 (Jun-Jul, 2013).
8. C. Molle *et al.*, Tristetraprolin regulation of interleukin 23 mRNA stability prevents a spontaneous inflammatory disease. *J Exp Med* **210**, 1675 (Aug 26, 2013).
9. E. Carballo, W. S. Lai, P. J. Blackshear, Feedback inhibition of macrophage tumor necrosis factor-alpha production by tristetraprolin. *Science* **281**, 1001 (Aug 14, 1998).
10. R. J. Rounbehler *et al.*, Tristetraprolin impairs myc-induced lymphoma and abolishes the malignant state. *Cell* **150**, 563 (Aug 3, 2012).
11. D. J. Hodson *et al.*, Deletion of the RNA-binding proteins ZFP36L1 and ZFP36L2 leads to perturbed thymic development and T lymphoblastic leukemia. *Nature immunology* **11**, 717 (Aug, 2010).
12. J. W. Zhu *et al.*, E2F1 and E2F2 determine thresholds for antigen-induced T-cell proliferation and suppress tumorigenesis. *Mol Cell Biol* **21**, 8547 (Dec, 2001).
13. T. Oki *et al.*, A novel cell-cycle-indicator, mVenus-p27K-, identifies quiescent cells and visualizes G0-G1 transition. *Scientific reports* **4**, 4012 (2014).
14. I. Huppertz *et al.*, iCLIP: protein-RNA interactions at nucleotide resolution. *Methods* **65**, 274 (Feb, 2014).
15. N. Mukherjee *et al.*, Global target mRNA specification and regulation by the RNA-binding protein ZFP36. *Genome biology* **15**, R12 (Jan 8, 2014).
16. D. Morishita, R. Katayama, K. Sekimizu, T. Tsuruo, N. Fujita, Pim kinases promote cell cycle progression by phosphorylating and down-regulating p27Kip1 at the transcriptional and posttranscriptional levels. *Cancer Res* **68**, 5076 (Jul 1, 2008).
17. R. J. Sheaff, M. Groudine, M. Gordon, J. M. Roberts, B. E. Clurman, Cyclin E-CDK2 is a regulator of p27Kip1. *Genes Dev* **11**, 1464 (Jun 1, 1997).
18. J. D. Keene, RNA regulons: coordination of post-transcriptional events. *Nature reviews. Genetics* **8**, 533 (Jul, 2007).
19. N. Herranz *et al.*, mTOR regulates MAPKAPK2 translation to control the senescence-associated secretory phenotype. *Nat Cell Biol* **17**, 1205 (Sep, 2015).
20. K. Ochiai *et al.*, A self-reinforcing regulatory network triggered by limiting IL-7 activates pre-BCR signaling and differentiation. *Nat Immunol* **13**, 300 (Mar, 2012).
21. A. B. Cooper *et al.*, A unique function for cyclin D3 in early B cell development. *Nat Immunol* **7**, 489 (May, 2006).
22. B. J. Thompson *et al.*, DYRK1A controls the transition from proliferation to quiescence during lymphoid development by destabilizing Cyclin D3. *J Exp Med* **212**, 953 (Jun 1, 2015).
23. M. Marderosian *et al.*, Tristetraprolin regulates Cyclin D1 and c-Myc mRNA stability in response to rapamycin in an Akt-dependent manner via p38 MAPK signaling. *Oncogene* **25**, 6277 (Oct 12, 2006).

24. D. J. Stumpo *et al.*, Targeted disruption of Zfp36l2, encoding a CCCH tandem zinc finger RNA-binding protein, results in defective hematopoiesis. *Blood* **114**, 2401 (Sep 17, 2009).
25. M. A. Hausburg *et al.*, Post-transcriptional regulation of satellite cell quiescence by TTP-mediated mRNA decay. *eLife* **4**, e03390 (2015).
26. A. S. Halees, R. El-Badrawi, K. S. Khabar, ARED Organism: expansion of ARED reveals AU-rich element cluster variations between human and mouse. *Nucleic Acids Res* **36**, D137 (Jan, 2008).
27. G. Yao, T. J. Lee, S. Mori, J. R. Nevins, L. You, A bistable Rb-E2F switch underlies the restriction point. *Nat Cell Biol* **10**, 476 (Apr, 2008).
28. D. Resnitzky, S. I. Reed, Different roles for cyclins D1 and E in regulation of the G1-to-S transition. *Molecular and cellular biology* **15**, 3463 (Jul, 1995).
29. E. Vigo *et al.*, CDC25A phosphatase is a target of E2F and is required for efficient E2F-induced S phase. *Molecular and cellular biology* **19**, 6379 (Sep, 1999).
30. G. Leone, J. DeGregori, L. Jakoi, J. G. Cook, J. R. Nevins, Collaborative role of E2F transcriptional activity and G1 cyclin dependent kinase activity in the induction of S phase. *Proceedings of the National Academy of Sciences of the United States of America* **96**, 6626 (Jun 8, 1999).
31. A. C. Minella *et al.*, Cyclin E phosphorylation regulates cell proliferation in hematopoietic and epithelial lineages in vivo. *Genes Dev* **22**, 1677 (Jun 15, 2008).
32. Y. Sasaki *et al.*, Canonical NF-kappaB activity, dispensable for B cell development, replaces BAFF-receptor signals and promotes B cell proliferation upon activation. *Immunity* **24**, 729 (Jun, 2006).
33. J. de Boer *et al.*, Transgenic mice with hematopoietic and lymphoid specific expression of Cre. *Eur. J. Immunol.* **33**, 314 (Feb, 2003).
34. E. Hobeika *et al.*, Testing gene function early in the B cell lineage in mb1-cre mice. *Proceedings of the National Academy of Sciences of the United States of America* **103**, 13789 (Sep 12, 2006).
35. T. G. Phan *et al.*, B cell receptor-independent stimuli trigger immunoglobulin (Ig) class switch recombination and production of IgG autoantibodies by anergic self-reactive B cells. *The Journal of experimental medicine* **197**, 845 (Apr 7, 2003).
36. A. Strasser *et al.*, Abnormalities of the immune system induced by dysregulated bcl-2 expression in transgenic mice. *Curr Top Microbiol Immunol* **166**, 175 (1990).
37. D. J. Bolland, M. R. King, W. Reik, A. E. Corcoran, C. Krueger, Robust 3D DNA FISH using directly labeled probes. *Journal of visualized experiments : JoVE*, (2013).
38. J. Konig *et al.*, iCLIP reveals the function of hnRNP particles in splicing at individual nucleotide resolution. *Nat Struct Mol Biol* **17**, 909 (Jul, 2010).
39. G. W. Yeo *et al.*, An RNA code for the FOX2 splicing regulator revealed by mapping RNA-protein interactions in stem cells. *Nat Struct Mol Biol* **16**, 130 (Feb, 2009).
40. S. Anders, W. Huber, Differential expression analysis for sequence count data. *Genome Biol* **11**, R106 (2010).
41. J. Chen, E. E. Bardes, B. J. Aronow, A. G. Jegga, ToppGene Suite for gene list enrichment analysis and candidate gene prioritization. *Nucleic Acids Res* **37**, W305 (Jul, 2009).
42. F. Sievers *et al.*, Fast, scalable generation of high-quality protein multiple sequence alignments using Clustal Omega. *Mol Syst Biol* **7**, 539 (2011).
43. K. Johnson *et al.*, Regulation of immunoglobulin light-chain recombination by the transcription factor IRF-4 and the attenuation of interleukin-7 signaling. *Immunity* **28**, 335 (Mar, 2008).
44. L. Dolken *et al.*, Systematic analysis of viral and cellular microRNA targets in cells latently infected with human gamma-herpesviruses by RISC immunoprecipitation assay. *Cell host & microbe* **7**, 324 (Apr 22, 2010).
45. J. T. Rodgers *et al.*, mTORC1 controls the adaptive transition of quiescent stem cells from G0 to G(Alert). *Nature* **510**, 393 (Jun 19, 2014).
46. T. A. Venezia *et al.*, Molecular signatures of proliferation and quiescence in hematopoietic stem cells. *PLoS Biol* **2**, e301 (Oct, 2004).

47. G. D. Victora *et al.*, Germinal center dynamics revealed by multiphoton microscopy with a photoactivatable fluorescent reporter. *Cell* **143**, 592 (Nov 12, 2010).
48. W. Shi *et al.*, Transcriptional profiling of mouse B cell terminal differentiation defines a signature for antibody-secreting plasma cells. *Nat Immunol* **16**, 663 (Jun, 2015).
49. J. A. Best *et al.*, Transcriptional insights into the CD8(+) T cell response to infection and memory T cell formation. *Nat Immunol* **14**, 404 (Apr, 2013).
50. A. P. Garner, C. R. Weston, D. E. Todd, K. Balmanno, S. J. Cook, Delta MEKK3:ER* activation induces a p38 alpha/beta 2-dependent cell cycle arrest at the G2 checkpoint. *Oncogene* **21**, 8089 (Nov 21, 2002).

Acknowledgements: We thank K. Vogel, R. Newman, C. Tiedje, and S. Bell for advice and comments on the manuscript; L. Matheson, A. Stark, and R. Venigalla for technical advice; and S. Bell, K. Bates, D. Sanger, N. Evans, and The Babraham Institute's Biological Support Unit, Flow Cytometry Core Facility, and Next Generation Sequencing Facility for expert technical assistance; J. Ule and T. Curk for help with iCLIP; L. Dolken for the gateway-compatible psi-check vector; and R. Brink, D. Kioussis and M. Reth for mice. This work was funded by the Biotechnology and Biological Sciences Research Council, a Medical Research Council CASE studentship with GSK, an MRC centenary award (A.G) and project grants from Bloodwise. DJH was supported by a Medical Research Council Clinician Scientist Fellowship. The data presented in this manuscript are tabulated in the main paper and in the supplementary materials. Sequencing data from the RNAseq and iCLIP experiments have been deposited in the NCBI Gene Expression Omnibus (GEO), and are accessible through GEO Series accession number GSE78249 (http://www.ncbi.nlm.nih.gov/geo/query/acc.cgi?acc=GSE78249). *Zfp36l1*^{fl}, *Zfp36l2*^{fl}, and *ROSA26*^{L1} mice are available from The Babraham Institute under a material transfer agreement.

[7] Sebastian Łukasiak's current address is: Wellcome Trust Sanger Institute Hinxton, Cambridge CB10 1SA, UK.

[8]Sara Ciullini Mannurita's current address is: Department of Neuroscience, Psychology, Pharmacology and Child Health (NEUROFARBA), Section of Child Health University of Florence-A. Meyer Children's Hospital Florence, Italy.

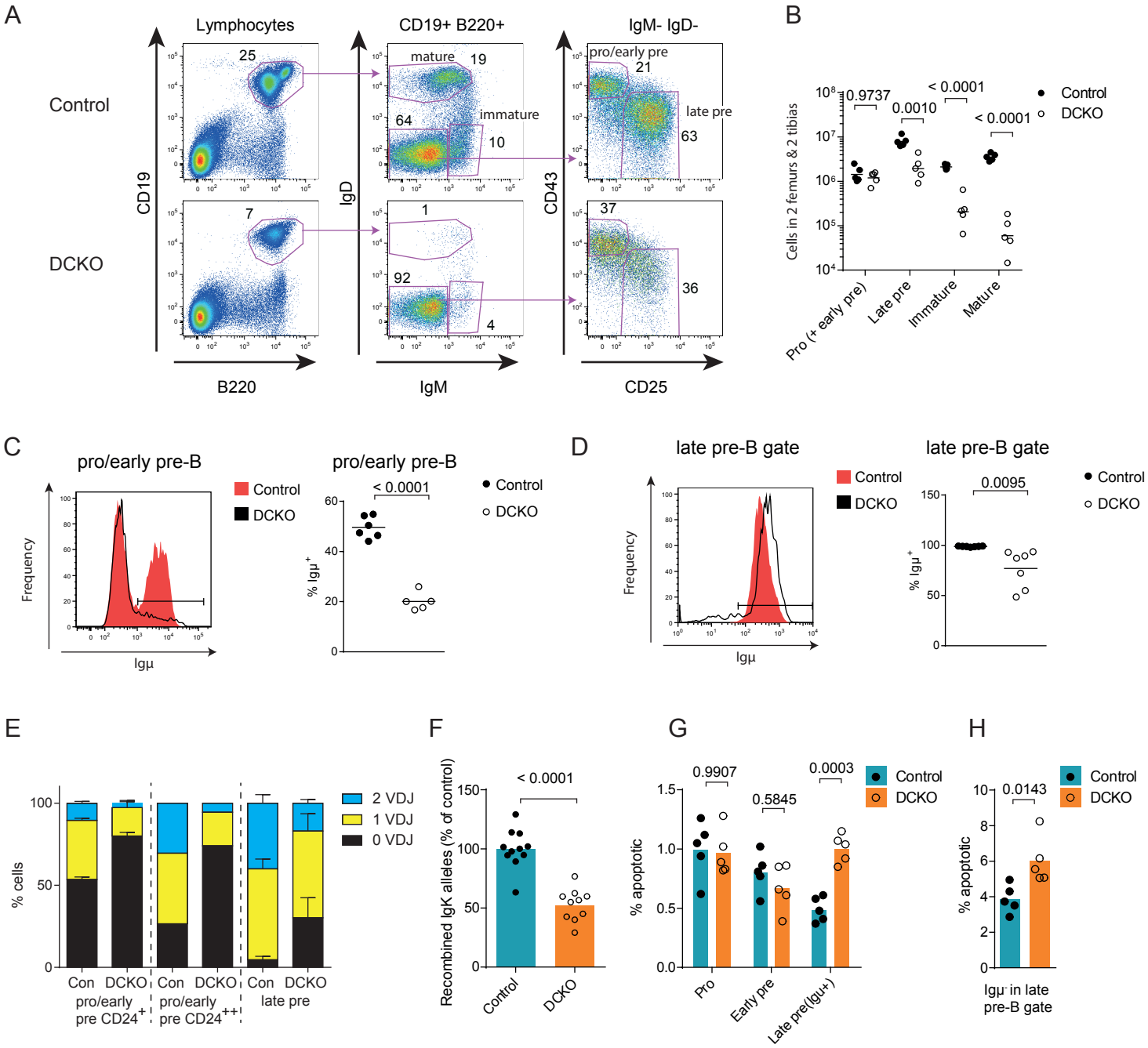
A
Lymphocytes
CD19+ B220+
IgM- IgD-
Control
DCKO
CD19
B220
IgD
IgM
CD43
CD25
25
7
mature
19
64
immature
10
1
92
4
pro/early pre
21
late pre
63
37
36
B
Cells in 2 femurs & 2 tibias
0.9737
0.0010
< 0.0001
< 0.0001
Control
DCKO
Pro (+ early pre)
Late pre
Immature
Mature
C
pro/early pre-B
Control
DCKO
Frequency
Igμ
< 0.0001
% Igμ+
D
late pre-B gate
0.0095
E
% cells
2 VDJ
1 VDJ
0 VDJ
Con pro/early pre CD24+
DCKO pro/early pre CD24+
Con late pre
DCKO late pre
F
Recombined IgK alleles (% of control)
< 0.0001
G
% apoptotic
0.9907
0.5845
0.0003
Pro
Early pre
Late pre(Igμ+)
H
0.0143
Igμ- in late pre-B gate

Figure 1

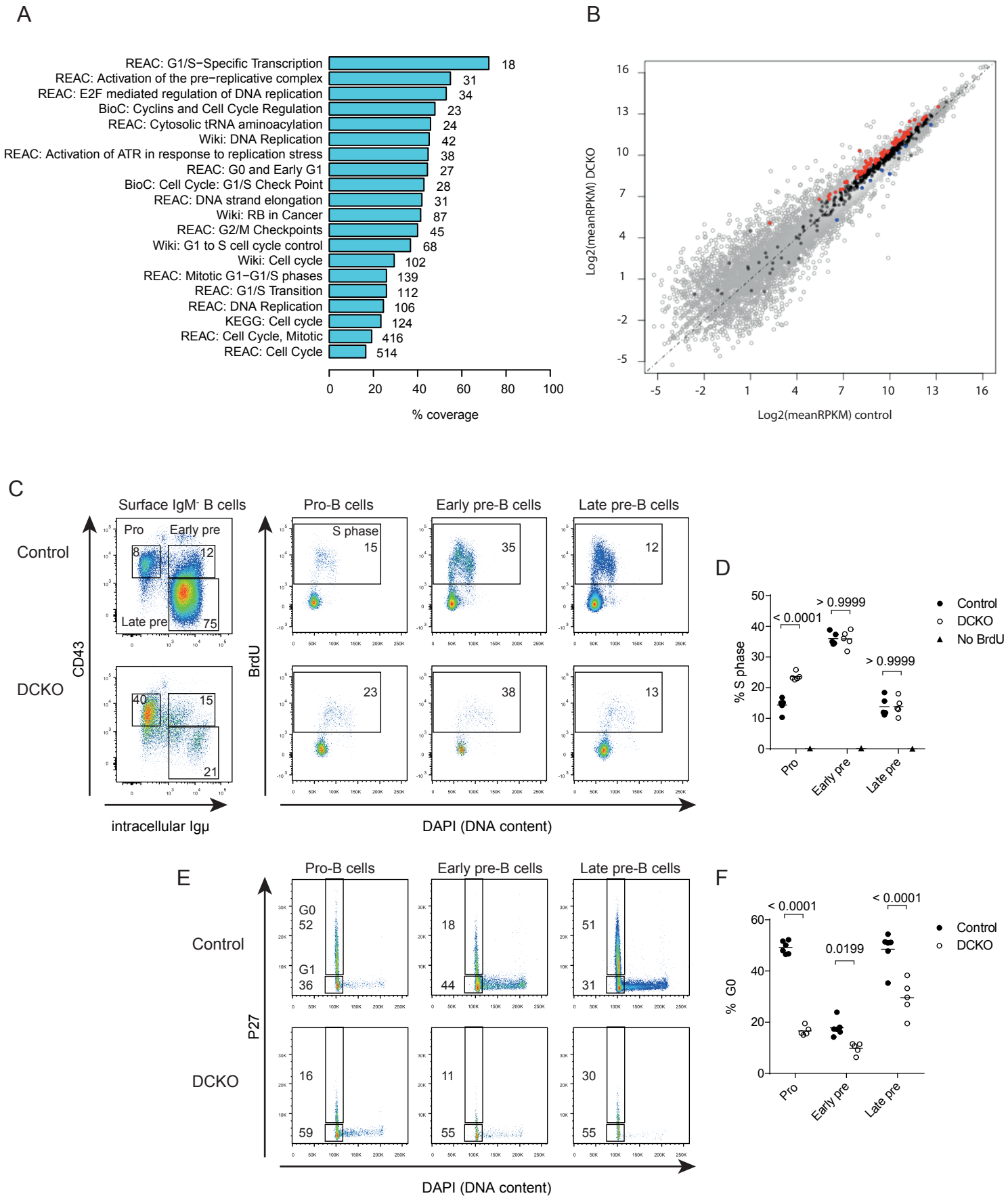
A
REAC: G1/S−Specific Transcription 18
REAC: Activation of the pre−replicative complex 31
REAC: E2F mediated regulation of DNA replication 34
BioC: Cyclins and Cell Cycle Regulation 23
REAC: Cytosolic tRNA aminoacylation 24
Wiki: DNA Replication 42
REAC: Activation of ATR in response to replication stress 38
REAC: G0 and Early G1 27
BioC: Cell Cycle: G1/S Check Point 28
REAC: DNA strand elongation 31
Wiki: RB in Cancer 87
REAC: G2/M Checkpoints 45
Wiki: G1 to S cell cycle control 68
Wiki: Cell cycle 102
REAC: Mitotic G1−G1/S phases 139
REAC: G1/S Transition 112
REAC: DNA Replication 106
KEGG: Cell cycle 124
REAC: Cell Cycle, Mitotic 416
REAC: Cell Cycle 514
0 20 40 60 80 100
% coverage
B
Log2(meanRPKM) DCKO
Log2(meanRPKM) control
C
Surface IgM- B cells
Pro-B cells
Early pre-B cells
Late pre-B cells
Control
DCKO
Pro
Early pre
Late pre
S phase
CD43
BrdU
intracellular Igμ
DAPI (DNA content)
D
% S phase
< 0.0001
> 0.9999
> 0.9999
Control
DCKO
No BrdU
E
G0
G1
P27
F
% G0
< 0.0001
0.0199
< 0.0001

Figure 2

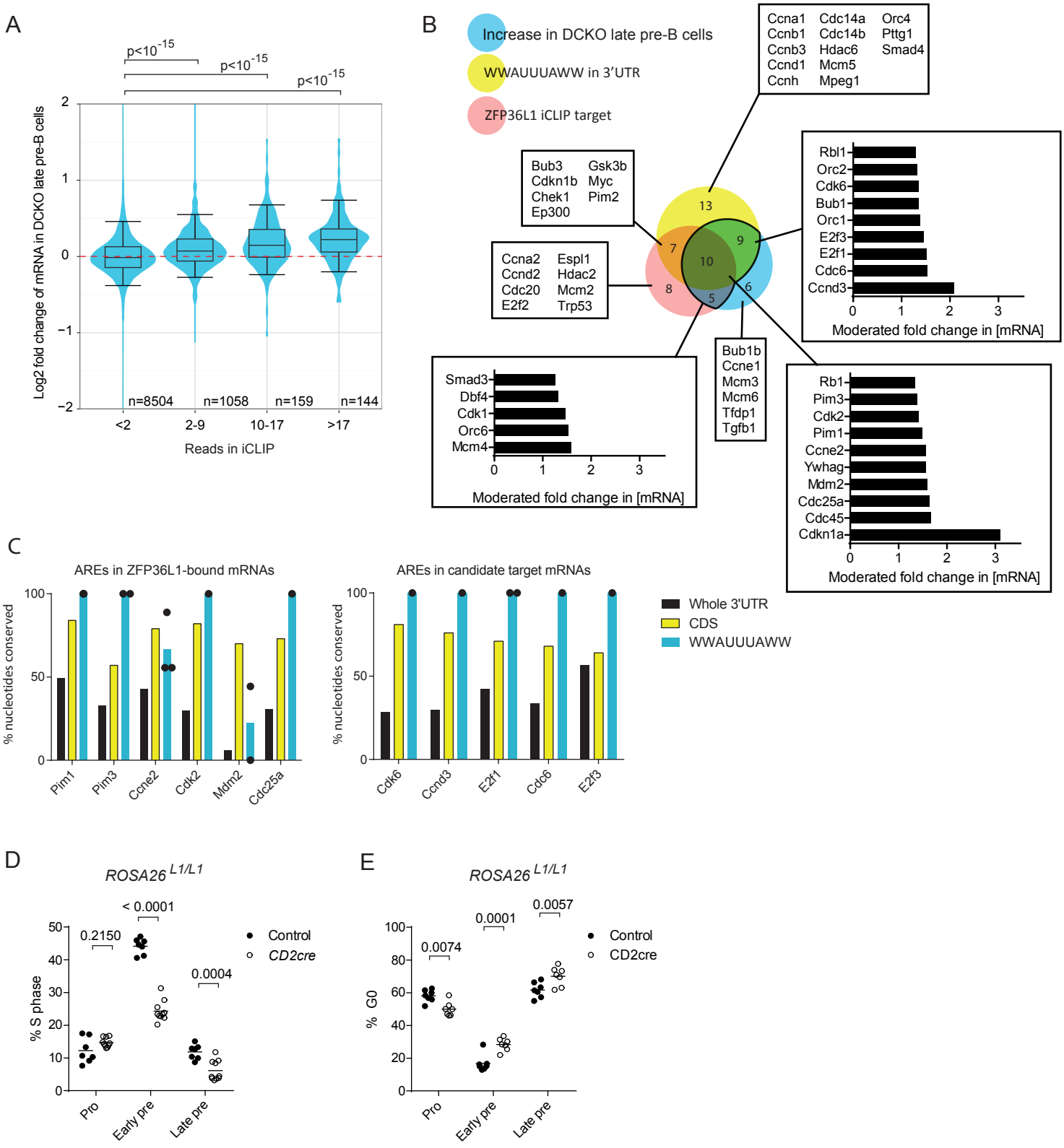
A
p<10-15
p<10-15
p<10-15
Log2 fold change of mRNA in DCKO late pre-B cells
n=8504
n=1058
n=159
n=144
<2
2-9
10-17
>17
Reads in iCLIP
B
Increase in DCKO late pre-B cells
WWAUUUAWW in 3'UTR
ZFP36L1 iCLIP target
Ccna1 Cdc14a Orc4
Ccnb1 Cdc14b Pttg1
Ccnb3 Hdac6 Smad4
Ccnd1 Mcm5
Ccnh Mpeg1
Bub3 Gsk3b
Cdkn1b Myc
Chek1 Pim2
Ep300
Ccna2 Espl1
Ccnd2 Hdac2
Cdc20 Mcm2
E2f2 Trp53
Bub1b
Ccne1
Mcm3
Mcm6
Tfdp1
Tgfb1
Rbl1
Orc2
Cdk6
Bub1
Orc1
E2f3
E2f1
Cdc6
Ccnd3
Moderated fold change in [mRNA]
Smad3
Dbf4
Cdk1
Orc6
Mcm4
Moderated fold change in [mRNA]
Rb1
Pim3
Cdk2
Pim1
Ccne2
Ywhag
Mdm2
Cdc25a
Cdc45
Cdkn1a
Moderated fold change in [mRNA]
C
AREs in ZFP36L1-bound mRNAs
AREs in candidate target mRNAs
% nucleotides conserved
Pim1
Pim3
Ccne2
Cdk2
Mdm2
Cdc25a
Cdk6
Ccnd3
E2f1
Cdc6
E2f3
Whole 3'UTR
CDS
WWAUUUAWW
D
ROSA26 L1/L1
< 0.0001
0.2150
0.0004
% S phase
Control
CD2cre
Pro
Early pre
Late pre
E
ROSA26 L1/L1
0.0057
0.0001
0.0074
% G0
Control
CD2cre
Pro
Early pre
Late pre

Figure 3

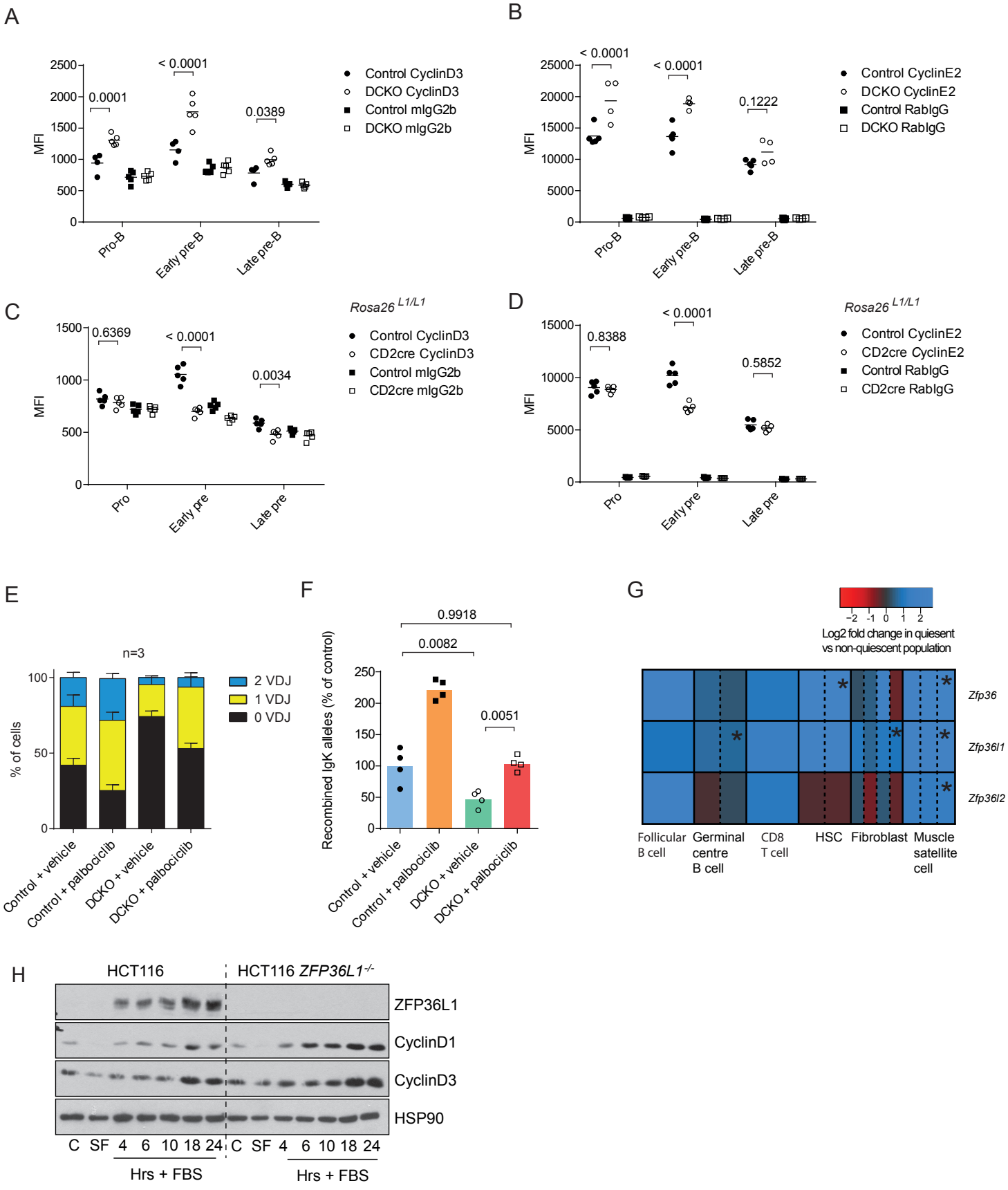
A
MFI
0.0001
< 0.0001
0.0389
Pro-B
Early pre-B
Late pre-B
Control CyclinD3
DCKO CyclinD3
Control mIgG2b
DCKO mIgG2b
B
< 0.0001
< 0.0001
0.1222
Control CyclinE2
DCKO CyclinE2
Control RabIgG
DCKO RabIgG
C
Rosa26 L1/L1
0.6369
< 0.0001
0.0034
Pro
Early pre
Late pre
Control CyclinD3
CD2cre CyclinD3
Control mIgG2b
CD2cre mIgG2b
D
Rosa26 L1/L1
0.8388
< 0.0001
0.5852
Control CyclinE2
CD2cre CyclinE2
Control RabIgG
CD2cre RabIgG
E
n=3
% of cells
2 VDJ
1 VDJ
0 VDJ
Control + vehicle
Control + palbociclib
DCKO + vehicle
DCKO + palbociclib
F
0.9918
0.0082
0.0051
Recombined IgK alleles (% of control)
G
Log2 fold change in quiesent vs non-quiescent population
Zfp36
Zfp36l1
Zfp36l2
Follicular B cell
Germinal centre B cell
CD8 T cell
HSC
Fibroblast
Muscle satellite cell
H
HCT116
HCT116 ZFP36L1-/-
ZFP36L1
CyclinD1
CyclinD3
HSP90
C SF 4 6 10 18 24
Hrs + FBS

Figure 4

Materials and Methods

Mice

All mice were housed in specific pathogen free IVC within the Babraham Institute Biological Support Unit. Breeding and experiments were performed using procedures approved after local ethical review and under the UK Animal (Scientific procedures) Act 1986.

Zfp36l1^{fl} mice (Zfp36l1$^{tm1.1Tnr}$) and *Zfp36l2*^{fl} mice (Zfp36l2$^{tm1.1Tnr}$) have been described previously (*11*). *ROSA26*^{L1} mice were generated using standard methods following targeting of the ROSA26 locus in Bruce4 (C57BL/6 origin) mouse embryonic stem cells with a targeting vector containing the cDNA encoding an N-terminal fusion of eGFP to human *ZFP36L1*. The parental targeting vector was generated by Klaus Rajewsky's laboratory (*32*). Two independently targeted ES cell lines were used to generate mice. The transgenes used for cell type specific Cre expression were *CD2cre* (Tg(CD2-cre)4Kio) (*33*) provided by Dimitris Koiussis ,and *Mb1*^{cre} (CD79a$^{tm1(cre)Reth}$) (*34*) provided by Michael Reth. IgH^{tg} mice carried the Igh^{tm1Rbr} allele (*35*) and were provided by Robert Brink. The BCL2 transgenic mice (C57BL/6-Tg(BCL2)36Wehi/J) were generated by S. Cory (*36*). Mouse strains were maintained on a C57BL/6 background.

Mice were genotyped using primers described in table S9.

Palbociclib administration

Palbociclib (Selleck Chemicals) was dissolved in 50mM sodium lactate (Sigma) and administered to mice by oral gavage daily for two or four days at a dose of 150mg/kg. Mice were culled and analyzed 1 day after the final administration of palbociclib.

NOTCH1 blocking antibody administration

Notch1-blocking antibody was administered as previously described (*11*) by intraperitoneal injection twice weekly for 3 weeks at a dose of 5 mg/kg.

Flow cytometry

Antibodies used are listed in tables S10, S11 and S12. The secondary antibody against mouse IgG2b was labelled using an Alexa Fluor 647 Antibody Labeling Kit from Molecular Probes (Life Technologies) according to the manufacturer's instructions. Bone marrow cells were flushed from the femurs and tibias and a cell suspension generated by pipetting and passing through a 40μm filter. Phosphate buffered saline (PBS) + 0.5% fetal calf serum (FCS) was used as FACS buffer. Cells were counted using a CASY counter (Schärfe systems/Roche).

For surface stains cells were incubated with Fc block (clone 2.4G2 from BioXcell) and antibodies in FACS buffer for 40 mins at 4°C and washed in FACS buffer. Where secondary antibodies or streptavidin were used these steps were repeated. Dead cell exclusion was achieved by suspending cells in 0.1μg/ml DAPI or using eFluor 780 fixable viability dye (eBioscience).

To stain for intracellular proteins, cells were first stained for surface markers then fixed in Becton Dickinson (BD) cytofix/cytoperm on ice for 30 mins, washed in perm/wash buffer (BD) and frozen at -80°C in 90% FCS 10% DMSO. After thawing, staining and washing of the cells was carried out using perm/wash buffer. Incubations with primary antibodies were carried out for one hour at room temperature and incubations with secondary antibodies, where necessary, were carried out for half an hour at 4°C. Where appropriate, DAPI was used to measure DNA content at a concentration of 1µg/ml.

For cell cycle analysis using BrdU mice were injected intraperitoneally with 1mg of BrdU (Sigma) dissolved in PBS then culled 2.5 hours later. The cells were stained for surface markers then fixed and stained for BrdU using a FITC or APC BrdU flow kit from BD according to the manufacturer's instructions.

Cells were stained for activated caspases using the CaspGLOW pan caspases kit (Biovision) according to the manufacturer's instructions. Incubation with FITC-VAD-FMK was carried out for one hour at 37°C in DMEM media (Life Technologies) supplemented with 10% FCS and 50µM β-mercaptoethanol (Sigma), and cells were subsequently stained with antibodies as described above.

Data was collected on an LSRII or Fortessa (BD) flow cytometer and analyzed using Flowjo software (Treestar).

Cell sorting was undertaken using a FACS Aria or Influx FACS sorter (BD). Bone marrow was depleted of red blood cells, macrophages and NK cells using MACS cell separation (Miltenyi). Cells were incubated with biotinylated antibodies against TER-119, NK1.1 and CD11b for 15 mins at 4°C in FACS buffer, washed, then incubated in anti-biotin MACS magnetic beads (Miltenyi) for 20 mins at 4°C. Cells were washed, then loaded onto MACS LS columns, and the negative fraction collected. Late pre-B cells were sorted as $CD19^+$, IgM^-, $CD43^-$, $CD25^+$ cells, pro/early pre-B cells were sorted as $CD19^+$, IgM^-, $CD43^+$, $CD25^-$ cells.

Gating strategies

For cell enumeration and cell sorting, based on surface stains pro/early pre-B cells were gated as $CD19^+$, IgM^-, IgD^-, $CD43^+$ cells; late pre-B cells as $CD19^+$, IgM^-, IgD^-, $CD43^-$, $CD25^+$; immature B cells as $CD19^+$, IgM^+, IgD^-; and mature B cells as $CD19^+$, IgD^+. The only exception to this is in figure S2B where pre-B cells were defined as $B220^+$, IgM^-, $CD25^+$; immature B cells were defined as $B220^{low}$, IgM^+; and mature B cells were defined as $B220^{high}$, $IgM^{+.}$

When using intracellular Igµ to differentiate pro and early pre-B cells in stains measuring BrdU, p27, active caspase, cyclinD3 or cyclinE2; pro-B cells were defined as $CD19^+$, surface IgM^-, $CD43^+$, intracellular $Igµ^-$; early pre-B cells were defined as $CD19^+$, surface IgM^-, $CD43^+$, intracellular $Igµ^+$; and late pre-B cells were defined as $CD19^+$, surface IgM^-, $CD43^-$, intracellular $Igµ^+$.

RNA extraction and cDNA conversion

Cells were pelleted by centrifugation and lysed in Trizol reagent (Invitrogen), snap frozen on dry ice and stored overnight at -80°C. RNA was extracted from the lysate by phenol-chloroform extraction. The aqueous phase was collected and RNA was precipitated using

isopropanol with 20µg of glycogen (Ambion) then washed twice with ethanol. RNA was air dried then resuspended in DEPC treated water and the RNA concentration was determined by NanoDrop. RNA samples were stored at -80°C.

0.25µg of RNA was converted to cDNA. Contaminating genomic DNA was removed using RNAse free DNAse (Ambion), in Superscript first strand buffer (Invitrogen), with 0.01M DTT and RNasin (Promega), incubated at 37°C for 15 mins. DNAse was heat inactivated at 70°C for 10 mins. Then cDNA was synthesized by using Superscript II reverse transcriptase (Invitrogen), with either 2.5µM random hexamers (Roche) (for evaluation of Zfp36 family expression) or 10ng/µl oligo dT (for evaluation of cell cycle regulator expression) for priming and 0.5µM dNTPS (Bioline). Reverse transcription was carried out by incubating at room temperature for 10 mins, 42°C for 40 mins then 70°C for 15 mins cDNA was diluted in 150µl DEPC treated water and stored at -20°C.

Genomic DNA isolation

Genomic DNA was isolated using the Gentra Puregene DNA isolation kit (Qiagen), according to the manufacturer's instructions. Following precipitation, samples were resuspended in Tris-EDTA buffer and stored at 4°C.

DNA-FISH

DNA FISH was performed as previously described (*37*) using *Igh* constant region BAC RP24-258E20, labelled with Alexa fluor 488, and a set of 7 plasmids containing non-repetitive parts of the V_H-D_H intergenic region (inserts sizes 1-3kb, ~15kb in total, sequences available on request), labelled with Alexa fluor 555. Signals were counted manually on an Olympus BX61 epifluorescence microscope system.

Mature B cell isolation and stimulation

B cells were isolated from mouse lymph nodes. Cells were incubated with biotinylated antibodies against CD5, CD43, CD11b and Ter119 for 30 mins on ice then washed and incubated in streptavidin-Dynabeads (Life Technologies) in PBS + 5% BSA for 15 mins on ice. Labelled cells were removed using a Dynabeads magnet for 5 mins at 4°C. The incubation with Dynabeads and magnetic separation was then repeated. The B cells were then plated at 2 million per ml in RPMI-1640 (Sigma) + 10% FCS + GlutaMAX (Gibco) + 100 U/ml Penicillin/Streptomycin (Life Technologies) + 50µM β-mercaptoethanol (Sigma) + 1mM Na-Pyruvate (Life Technologies) + 10µg/ml LPS (Sigma) + 10ng/ml IL4 (PeproTech) + 5ng/ml IL5 (Sigma) for 48 hours at 37°C 5% CO_2.

Preparation of protein lysates for Individual-nucleotide resolution Cross-Linking and ImmunoPrecipitation (iCLIP).

After washing with ice-cold PBS, intact cells were irradiated with UV-light (300 mJ/cm^2, Stratalinker 2400) then lysed in lysis buffer (50mM Tris HCl, pH 8.0, 100mM NaCl, 1% NP-40, 0.5% deoxycholate, 0.1% SDS, 1:200 protease inhibitor cocktail (Sigma). The lysates were

sonicated then protein was quantitated using a BCA assay kit (Thermo Scientific Pierce) by comparison to a serial dilution of albumin.

Immunoprecipitation and resolution of ZFP36L1-RNA complexes

Rabbit anti-ZFP36L1 antibody (Brf1/2 from Cell Signaling) was conjugated to Protein A-Dynabeads (Invitrogen) to make Brf1/2-Dynabeads. iCLIP experiments were performed essentially as described previously (*38*). For each experiment 2mg of B cell protein supernatant was cleared by centrifugation then digested with TURBO DNAse (Ambion) and RNase I (Ambion) for 3 mins at 37°C. The lysates were then treated with SUPERase-In (Ambion) to stop the RNAse digestion.

Immunoprecipitation was performed using Brf1/2-Dynabeads for 4.5 hours at 4°C. The beads were then washed in high stringency buffer (50 mM Tris-HCl, pH 7.4, 1M NaCl, 1 mM EDTA, 1% NP-40, 0.6% SDS, 0.3% Sodium deoxycholate), then in PNK wash (20 mM Tris-HCl, pH 7.4, 10 mM $MgCl_2$, 0.2% Tween-20). RNA dephosphorylation was carried out in PNK buffer (NEB) with RNAsin (NEB) and PNK (NEB) at 37°C for 20 minutes. Beads were then washed in low stringency buffer (50 mM Tris-HCl, pH 7.4, 1M NaCl, 1mM EDTA, 1% NP-40, 0.2% SDS, 0.5% Sodium deoxycholate). All subsequent steps were done exactly as described in (*38*). cDNA libraries from four independent experiments were prepared and sequenced using Illumina's HiSeq2000 (100 bp single end sequencing). RCLIP primers used for RNA reverse transcription included a barcode at the 5'end with three known bases and four random nucleotides (table S13).

Bioinformatics analysis of iCLIP libraries.

iCLIP analysis was performed as previously described (*38*). Briefly, sample demultiplexing was performed by identification of the 3 known bases of the 7 bases barcode introduced in the 5' end of the read by the RCLIP primer. The remaining four random bases were used to remove PCR duplicate reads. Reads were trimmed to remove any adaptor sequence and barcodes before mapping reads to genome mm10 using Bowtie. After read mapping, the single-nucleotide at position -1 was annotated as unique ZFP36L1 crosslink site. Identification of highly significant ZFP36L1 binding sites was performed using iCount to assign a FDR to each crosslink site as previously described (*39*) with the following considerations. (i) The height associated to a unique ZFP36L1 crosslink site was calculated as the sum number of cDNA counts from four independent experiments. (ii) Windows were created by extending crosslink sites 15 nucleotides to both directions. (iii) 100 permutations were allowed to calculate the background frequency. Only ZFP36L1 crosslink sites with a FDR < 0.05 were further considered in our analysis. Cross link sites identified were analysed for KMER content in iCOUNT. All occurrences of an 8-nucleotide kmer in the windows -30nt to -10nt and 10nt to 30nt relative to each cross-link are counted. Random reference data was generated 100 times by random shuffling of iCLIP cross-link positions within corresponding genome segments (within the same genes).

RNAseq

RNAseq libraries were prepared from 0.1 µg of RNA from sorted control and DCKO late pre-B cells using TruSeq RNA sample preparation kit v2 modified to be strand specific using the dUTP method. Libraries were sequenced by an Illumina genome analyzer II measuring 54bp single-end reads. Over 30 million reads were measured from each sample. The reads were trimmed to remove adapter sequences using Trim Galore then mapped using Tophat (version 1.1.4) to the NCBI m37 mouse assembly (April 2007, strain C57BL/6J); reads with an identical sequence to more than one genomic locus were not mapped. Quality control analysis was carried out with Fast QC.

Differential expression of transcripts

Read counts for each gene were generated in SeqMonk: transcripts from the same gene were collapsed into a single transcript containing all exons, so total reads were counted without considering alternative splice forms. Since the libraries were strand-specific only reads on the opposing strand were counted. Differences in the abundance of transcripts between DCKO and control late pre-B cells were calculated in the R/Bioconductor program DESeq (version 1.12.1) (*40*) which fits read count data to a negative binomial distribution and uses a shrinkage estimator to estimate the distribution's variance. Adjusted P values for differential expression were calculated in DESeq using a Benjamini-Hochberg correction: genes with an adjusted p-value of less than 5% were considered significant.

Gene set enrichment analysis

Differentially expressed mouse transcripts identified using DESEQ, or iCLIP targets with at least two reads in the 3'UTR, were analyzed for gene set enrichment using Toppfun using a false discovery rate cut off of 0.05 (*41*). Pathway analysis included gene sets from Biocarta, Reactome, Wikipathways and Kegg databases. GO term analysis used the GO biological pathways database. Log2 transformed normalized mean gene counts divided by gene length (RPKM) for genes in the control and DCKO RNAseq datasets were plotted in R with indicated gene lists highlighted.

Expression of transcripts with RBP binding sites

To compare the expression of mRNAs depending on the presence of ZFP36L1 binding sites in their 3'UTRs the moderated log2 fold change between DCKO and control samples for each gene was calculated in DESeq from moderated expression values from the DESeq variance Stabilizing Transformation function. The 50% of genes with the greatest overall read counts between all samples were selected for analysis and the *Zfp36l1* and *Zfp36l2* genes were removed from the analysis. The genes were then grouped according to the number of ZFP36L1 iCLIP reads within significant peaks (FDR<5%) in the 3'UTR of each gene. Violin plots were drawn using ggplot2 in R, and the groups were compared by an ANOVA with Tukey's post-test in R.

Comparisons of the expression of mRNAs depending on the presence of AREs in their 3'UTRs was performed as per the comparison with ZFP36L1 binding sites except the number of

WWAUUUAWW motifs in each 3'UTR was used to group the genes. 3'UTR sequences were obtained from Ensembl through biomaRt (biomaRt version 2.16.0, Ensembl release 77) and the longest 3'UTR from each gene was considered. The number of WWAUUUAWW motifs in each 3'UTR were counted using BioStrings in R.

Comparisons of the expression of mRNAs depending on the presence of Zfp36 binding sites in the 3'UTRs of their human homologue was performed as per the comparison with ZFP36L1 binding sites except the number of Zfp36 binding sites determined by PAR-CLIP in human HEK293 cells was considered (*15*). A cut-off of at least four PAR-CLIP reads with C to T transitions within the 3'UTR was used to distinguish mRNAs with and without binding sites and genes were grouped according to the number of binding sites identified and were matched to their mouse homologue.

Regulation of cell cycle transcripts by ZFP36 family RBP

A gene list containing 90 cell cycle regulator mRNAs was used to prepare a Venn diagram showing the overlap between the presence of ZFP36L1 binding sites (defined by at least two iCLIP reads in the mRNA's 3'UTR), the presence of WWAUUUAWW motifs, and significant increases of mRNA in DCKO late pre-B cells. The data used in this comparison is shown in table S8. The Venn diagram was drawn using the venneuler package in R.

For the Venn diagram of cell cycle mRNAs showing the overlap between significant increases in mRNA in DCKO late pre-B cells and presence of Zfp36 binding sites in their human homologues identified by PAR-CLIP in HEK-293 cells a cut-off of at least four PAR-CLIP reads with C to T transitions within the 3'UTR was used to distinguish mRNAs with and without binding sites.

Analysis of sequence conservation in Zfp36 binding sites and AREs

Coding sequence (CDS) or 3'UTR sequences from the species indicated were aligned using Clustal Omega (*42*). Each nucleotide on the alignment was considered conserved if it matched across all six species. AU-rich elements were identified as any element matching the sequence WWATTTAWW in the mouse 3'UTR, then where nucleotides identified by iCLIP were outside of these sequences a seven nucleotide motif surrounding the identified nucleotide was considered, where these motifs overlapped they considered as a single longer motif.

qPCR

For TaqMan assays Platinum taq supermix with UDG (Invitrogen) was used with TaqMan probes and primers (Life Technologies) indicated in tables S14 and S15. For SybrGreen assays Platinum Taq SybrGreen supermix (Invitrogen) was used primers are described in table S16.

The abundance of *Zfp36l1* exon 2 and *Zfp36l2* exon 2 in genomic DNA was calculated using the $2^{\wedge\text{-dCT}}$ method with *Tbp* and *Zfp36l2* exon1 used as controls respectively. This was possible because the efficiency of the control assays was equal to that of the test assays.

Igκ recombination was measured as previously described (*43*). Kappa recombination products were normalized to total DNA using a product covering iEκ using the $2^{\wedge\text{-dCT}}$ method.

The RT-qPCR assays measuring transcript abundance were normalized to multiple controls. The relative abundance of each mRNA was calculated by referring to a standard dilution of cDNA.

Plasmids

PCDNA ZFP36L1 and ZFP36L1-tandem zinc finger mutant expression constructs were generated as described previously (*11*). Constructs containing CylinE2 3'UTR and mutant dARE CyclinE2 3'UTR flanked by gateway AttB-sites were generated by plasmid synthesis (Life Technologies). These were cloned into pDonor 221 (Life technologies) using BP clonase (Life technologies). The 3'UTR sequences were then cloned downstream of the firefly luciferase CDS in a gateway- compatible psi check vector (kindly provided by Lars Dolken) (*44*).

Luciferase assays to demonstrate the Ccne2 ARE is functional.

HELA cells were grown in DMEM (Life technologies), supplemented with 10% FCS (Life technologies), and penicillin/streptomycin (Life technologies). Psi-check and ZFP36L1-expression vectors were transfected into HELA cells using X-treme gene HP (Roche). Cells were harvested 48 hours after transfection, and renilla and firefly luciferase activities were assayed using the dual-luciferase reporter assay system (Promega) with a MicroLumatPlus LB96V luminometer (Berthold Technologies).

Analysis of Zfp36 family member expression in quiescent and non-quiescent cell populations

Publically available data for muscle satellite cells (GSE47177, Rodgers et al 2014 Nature (*45*)); hematopoietic stem cells (GSE1559, Venezia et al 2004 PLOS Biol (*46*)); NIH3T3 cells in G0 and G1 phases (GSE46511, Oki et al 2014 Nature (*13*)); germinal center B cells photoactivated in the light zone or dark zone (GSE23925, Victora et al 2010 Cell (*47*)); undivided resting and activated B cells (GSE60927, Shi et al 2015 Nat Immunol (*48*)); and resting and undivided OT-I CD8 T cells from mice infected with OVA-expressing *Listeria monocytogenes* (Lm-OVA) (GSE15907, Best et al 2013 Nat Immunol (*49*)) were downloaded from GEO. RNA-seq data was aligned to mouse genome (GRCm38) using TopHat and read counts were generated using HTSeq count. DESeq2 was used to calculate log2FC. Normalised signal values from microarray studies were log2 transformed and signal log ratio between conditions were calculated. Log2FC for each comparison were visualized using a heatmap in R.

Generation of *ZFP36L1*$^{-/-}$ HCT116 cells

Guide RNAs to human *ZFP36L1* were designed using Horizon Technology's Guidebook and cloned into their Cas9-expressing plasmids. HCT116 cells were transfected with the guide RNA-containing plasmids by electroporation using a nucleofector machine (Amaxa). Transfection was monitored by GFP expression and flow cytometry used to sort single GFP-positive cells into 96 well plates. Clones of interest were expanded and assessed for the presence or absence of ZFP36L1 by Western blot. Guide RNA

AACTATAGTGCTCCCAGTGC was successful in ablating ZFP36L1 expression in multiple independent clones.

Western blotting

Parental or *ZFP36L1*$^{-/-}$ HCT116 cells were seeded into 10cm dishes. Cells (60% confluent) were serum starved for 24 hours before re-stimulation with 10% FBS for the indicated times. Cells were lysed in ice cold TG lysis buffer (*50*) assayed for protein content, separated by SDS PAGE and transferred to PVDF membranes. The membranes were then blocked with 5% non-fat milk in TBST before overnight incubation at 4^{o}C with the indicated antibodies (table S10). Blots were then washed in TBST, incubated with HRP-conjugated secondary antibodies and results visualised with ECL.

Statistics

Except for data generated by high throughput sequencing, where statistical tests are described elsewhere, all statistical analyses were performed using prism software (GraphPad). The test used and sample sizes are indicated in the figure legends. When data were displayed on a logarithmic scale, log-transformed data were used in comparisons.

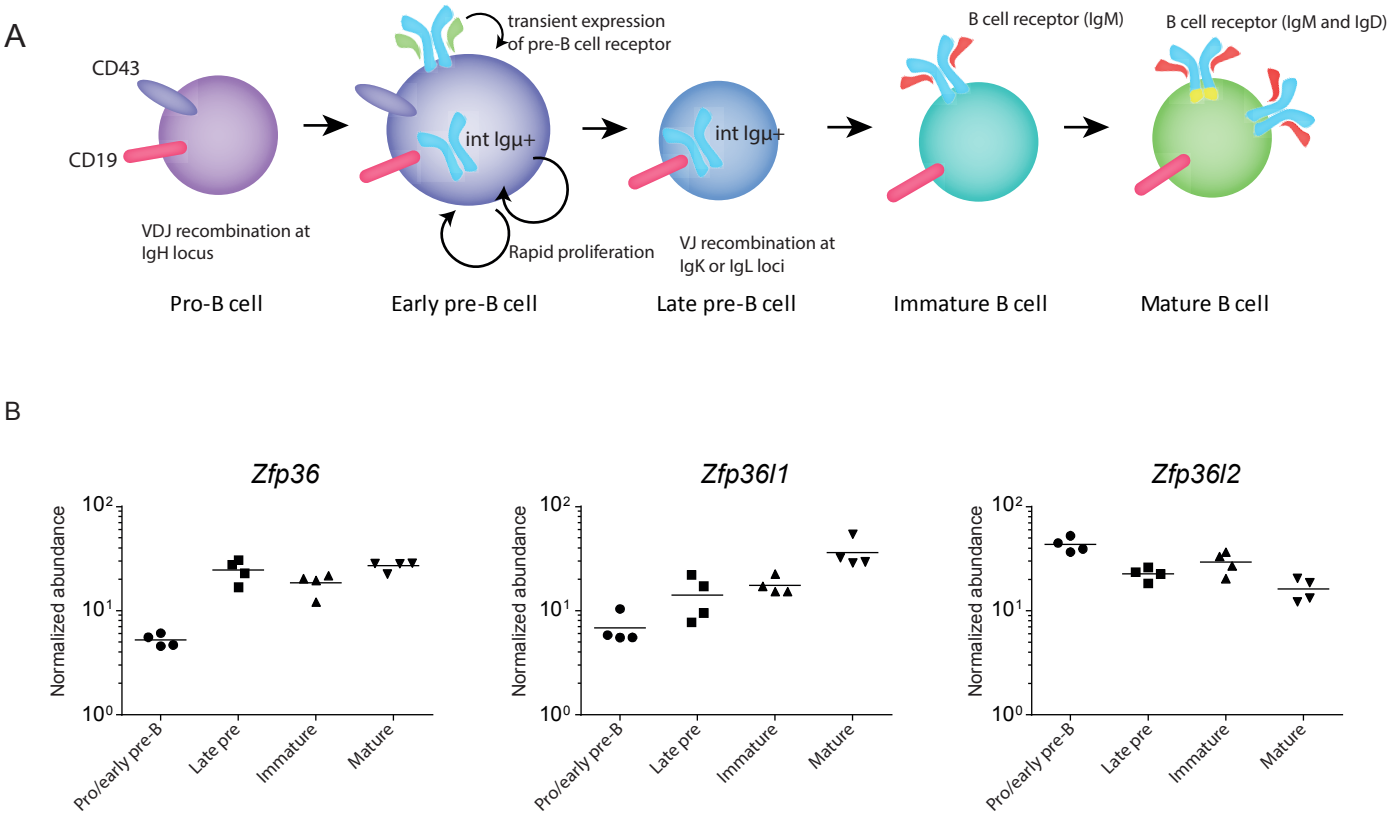

Fig. S1: Expression of Zfp36 family members through B cell development.
(A) Schematic depicting B cell developmental stages in the mouse bone marrow and indicating the markers used to identify cells at different stages. (B) RT-qPCR on sorted cells measuring the abundance of Zfp36 family mRNAs. Data is normalized to four reference genes: *Tbp*, *Hprt*, *Actb* and *B2m*. Four biological replicates are shown, data are from a single experiment.

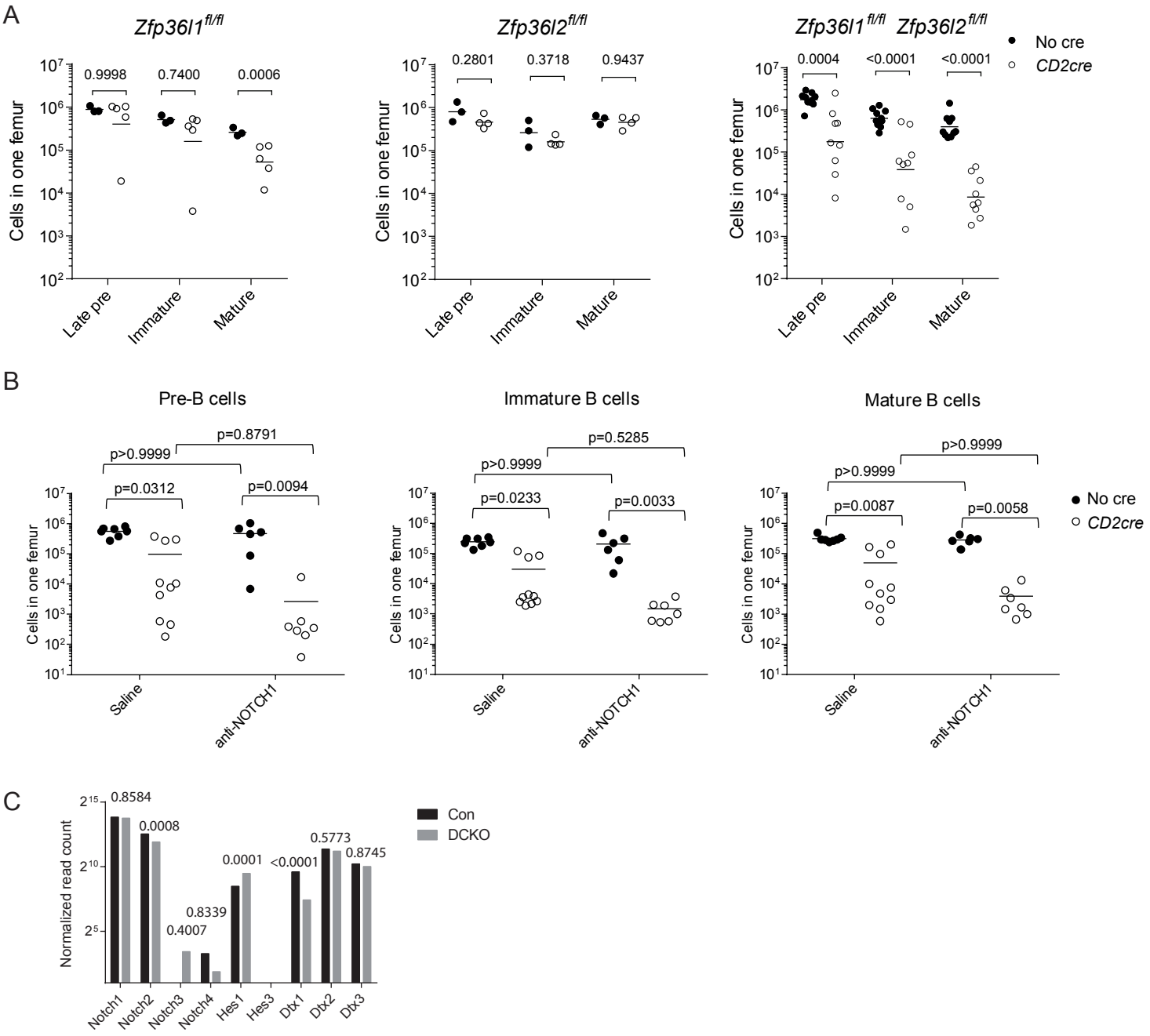

Fig. S2: Double conditional knockout of *Zfp36l1* and *Zfp36l2* abrogates early B cell development in a NOTCH1 independent manner.

(A) Flow cytometric quantification of bone marrow B cell developmental subsets in mice with single or double conditional knockout of *Zfp36l1* and *Zfp36l2* showing that knockout of *Zfp36l1* or *Zfp36l2* alone does not affect the earliest stages of B cell development, but knockout of both genes leads to reduced pre-B cell numbers. *Zfp36l1*$^{fl/fl}$ (n=3), *Zfp36l1*$^{fl/fl}$ *CD2cre* (n=5), *Zfp36l2*$^{fl/fl}$ (n=3), *Zfp36l2*$^{fl/fl}$ *CD2cre* (n=5), *Zfp36l1*$^{fl/fl}$ *Zfp36l2*$^{fl/fl}$ (n=10), and *Zfp36l1*$^{fl/fl}$ *Zfp36l2*$^{fl/fl}$ *CD2cre* (n=9) mice are shown. Data on *Zfp36l1*$^{fl/fl}$ and *Zfp36l2*$^{fl/fl}$ mice are representative of single experiments; data from *Zfp36l1*$^{fl/fl}$ *Zfp36l2*$^{fl/fl}$ mice are from two independent experiments. *CD2cre* and control populations were compared by an ANOVA with Sidak's post-test. Symbols indicate biological replicates, bars represent geometric means. (B) *Zfp36l1*$^{fl/fl}$ *Zfp36l2*$^{fl/fl}$ mice were injected intraperitoneally with 5ug/g of NOTCH1 blocking antibody twice weekly for three weeks, then the numbers of cells at B cell developmental stages quantified. This treatment caused the regression of thymic tumors in *Zfp36l1*$^{fl/fl}$ *Zfp36l2*$^{fl/fl}$ *CD2cre* mice (*11*), but did not rescue B cell development. Each symbol represents a biological replicate and lines represent the median value for each group. Results were analysed by a Kruskal-Wallis test with Dunn's post test for pairwise comparisons. (C) Abundance of NOTCH pathway mRNAs in control (n=3) and DCKO (*Zfp36l1*$^{fl/fl}$ *Zfp36l2*$^{fl/fl}$ *Mb1*$^{cre/+}$, n=2) late pre-B cells measured by RNAseq does not suggest any increase in the activity of this pathway in DCKOs. Adjusted p-values are shown.

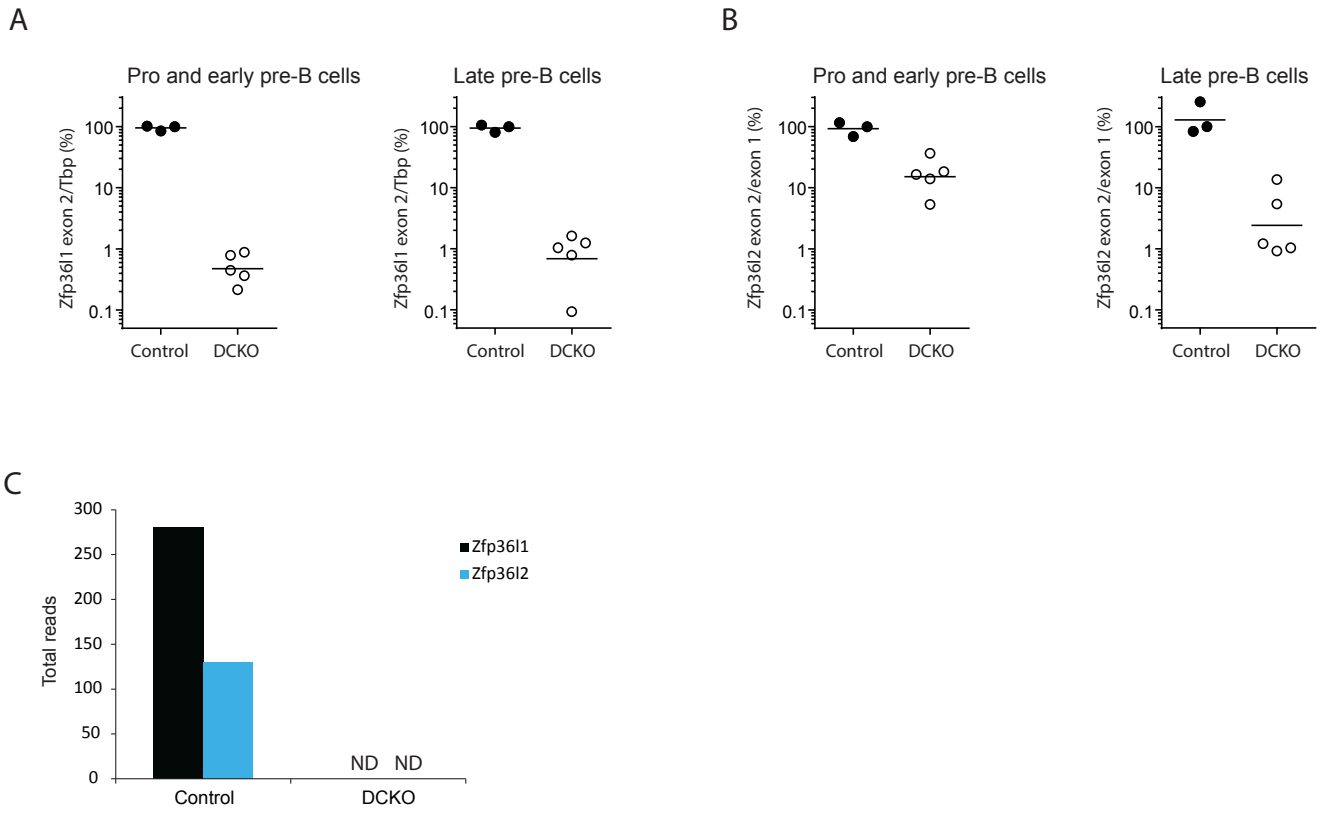

Fig. S3: *Zfp36l1*^{fl} and *Zfp36l2*^{fl} alleles are efficiently recombined by *Mb1*^{cre}.
(A, B) qPCR on DNA isolated from sorted control (n=3) and DCKO (n=5) pro- and pre-B cells to measure the relative abundance of an amplicon in the floxed region of *Zfp36l1* (A) and *Zfp36l2* (B). Data are from a single experiment. Symbols indicate biological replicates, bars represent the geometric means. (C) Number of RNAseq reads aligning to the CDS in exon 2 of *Zfp36l1* and *Zfp36l2* in libraries from sorted control (average of 3 replicates) and DCKO (average of two replicates) late pre-B cells. N.D. (not detected) indicates that no reads aligned to these regions in libraries from the DCKO late pre-B cells.

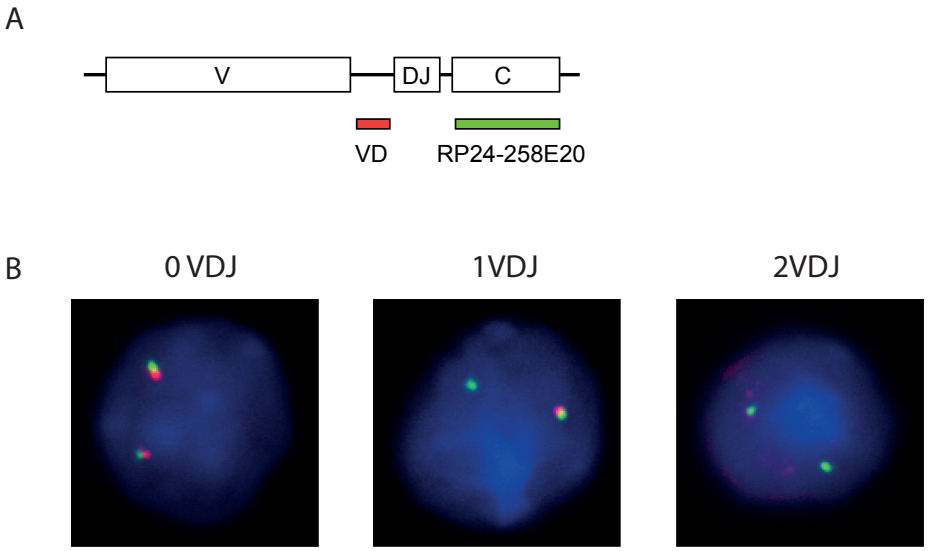

Fig. S4: DNA FISH to investigate recombination of the IgH loci.
(A) Schematic of probes used to detect regions of DNA corresponding to the C_H region and V_H-D_H intergenic region of the IgH locus. (B) Representative FISH images showing cells with zero, one or two V to DJ recombined IgH alleles.

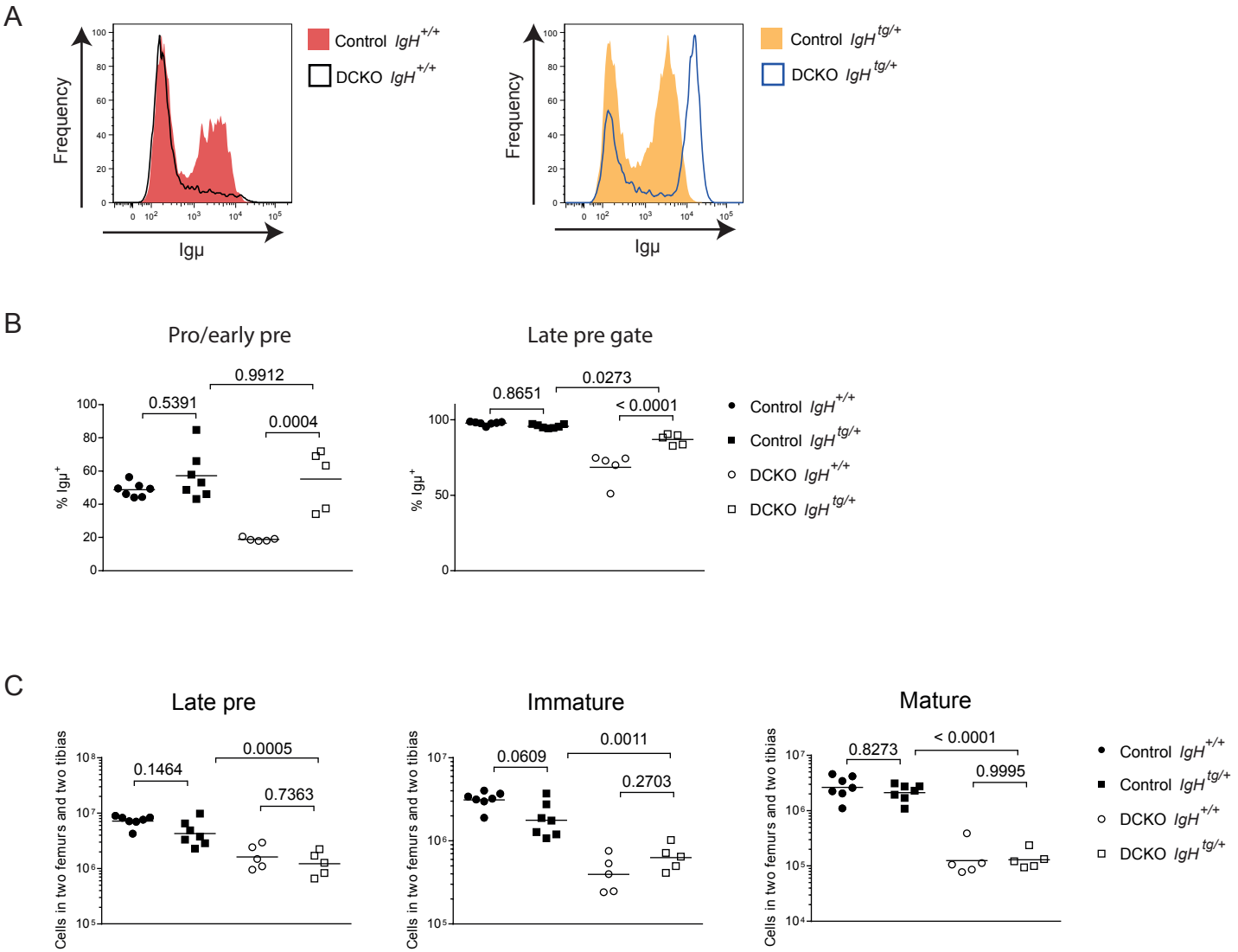

Fig. S5: SWHEL IgH transgene does not restore the numbers of pre-, immature-, or mature-B cells in DCKO *IgH*$^{tg/+}$ mice.
(A) Representative histograms showing flow cytometry of intracellular Igμ in control *IgH*$^{+/+}$, control *IgH*$^{tg/+}$, DCKO *IgH*$^{+/+}$, and DCKO *IgH*$^{tg/+}$ pro- and early pre-B cells. (B) Proportion of cells expressing intracellular Igμ within indicated bone marrow B cell subsets of control *IgH*$^{+/+}$ (n=7), control *IgH*$^{tg/+}$ (n=7), DCKO *IgH*$^{+/+}$ (n=5), and DCKO *IgH*$^{tg/+}$ (n=5) mice. These data show that Igμ expression is restored by the SWHEL IgH transgene at the early pre-B cell stage, but there is still aberrant selection of Igμ^{-} cells to the late pre-B cell stage. Data are from a single experiment. (C) Flow cytometric quantification of B cell developmental subsets in the bone marrow of control *IgH*$^{+/+}$ (n=7), control *IgH*$^{tg/+}$ (n=7), DCKO *IgH*$^{+/+}$ (n=5), and DCKO *IgH*$^{tg/+}$ (n=5) mice, demonstrating the SWHEL IgH transgene does not rescue cellularity at the late pre, immature or mature B cell stages. Data are from a single experiment. Populations were compared by an ANOVA with Sidak's post-test, symbols indicate biological replicates, bars represent means in (B) and geometric means in (C).

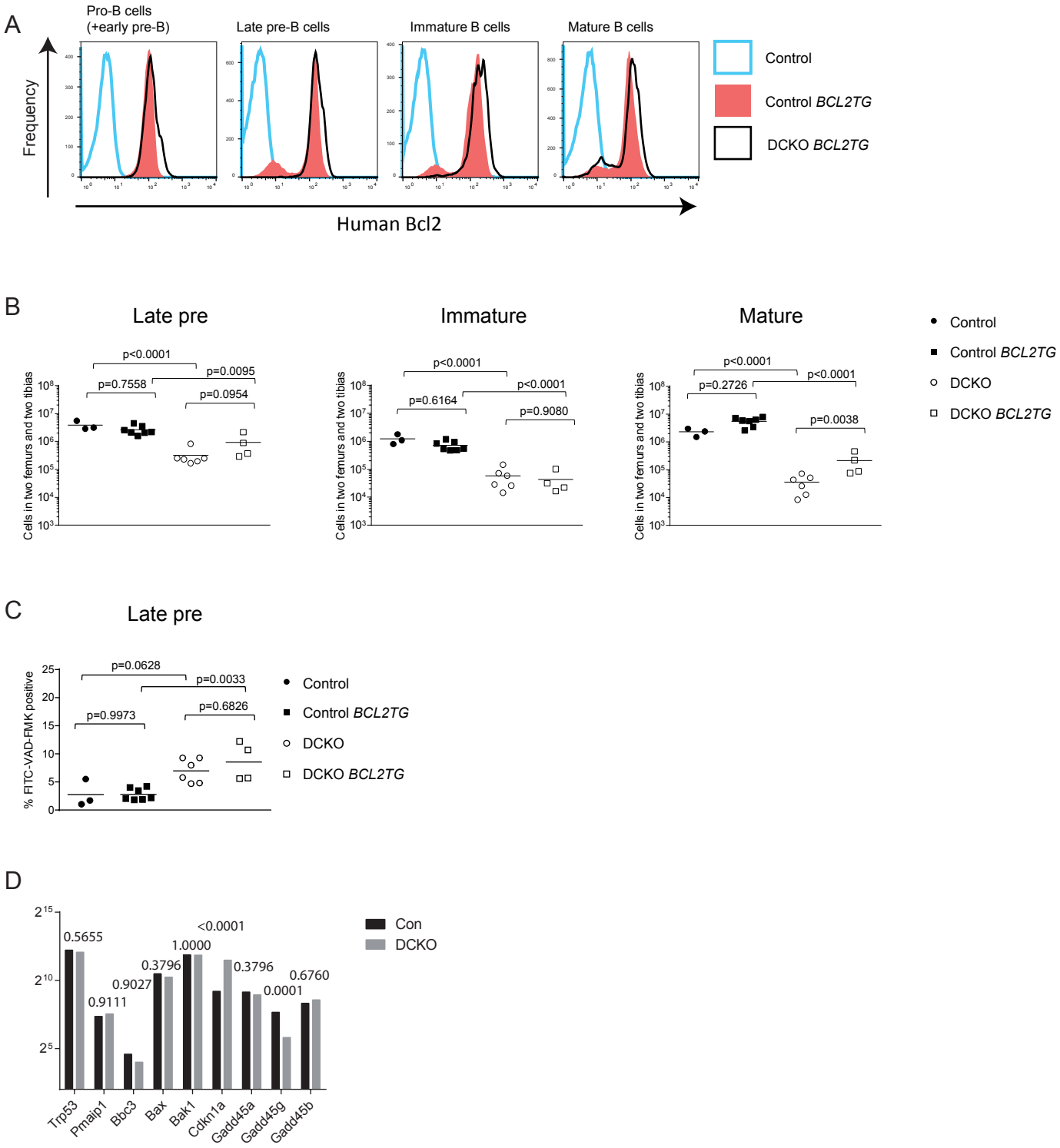

Fig. S6: Apoptosis of DCKO late pre-B cells cannot be rescued by expression of BCL2. (A) Representative FACS plots showing staining for human BCL2 in control (n=1), control *BCL2TG* (n=3), and DCKO *BCL2TG* (n=4) B cell progenitor populations. (B) Flow cytometric quantification of B cell developmental subsets in the bone marrow of control (n=3), control *BCL2TG* (n=7), DCKO (n=6), and DCKO *BCL2TG* (n=4) mice demonstrating no rescue of B cell development by the BCL2 transgene. Symbols indicate biological replicates, bars represent geometric means. (C) Proportion of control (n=3), control *BCL2TG* (n=7), DCKO (n=6), and DCKO *BCL2TG* (n=4) late pre-B cells in early apoptosis demonstrating the BCL2 transgene does not rescue apoptosis in DCKO late pre-B cells. Symbols indicate biological replicates, bars represent means, populations were compared by an ANOVA with Sidak's post-test. (D) Abundance of mRNAs that are involved in the P53 pathway in control (n=3) and DCKO (n=2) late pre-B cells measured by RNAseq demonstrating that we cannot detect a transcriptional signature indicative of increased P53 activity in the DCKO late pre-B cells. Notably Pmaip, Bbc3, Bax and Bak1 which directly induce apoptosis were unchanged in DCKOs. Adjusted p-values are shown.

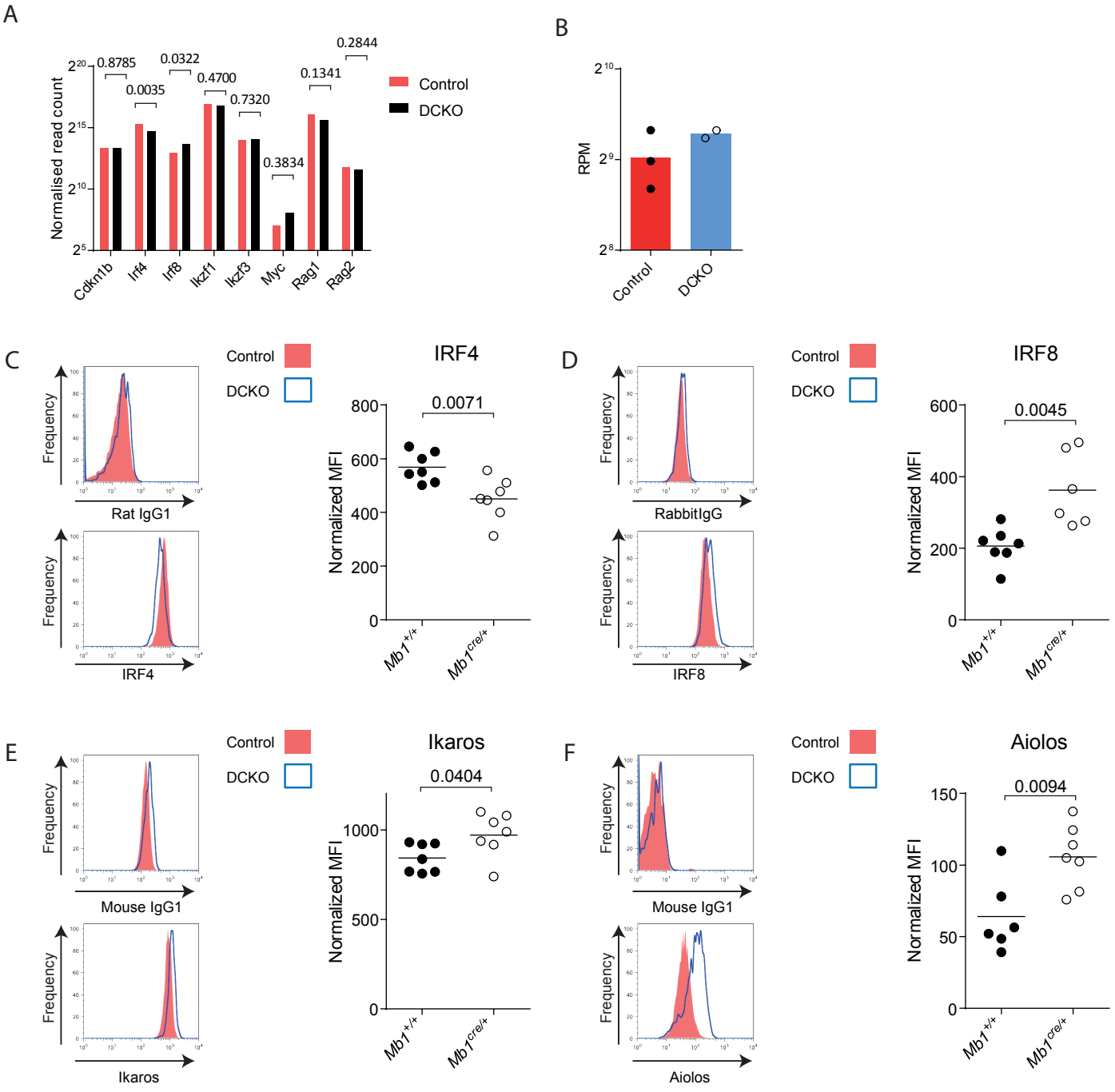

Fig. S7: Expression of mRNAs and proteins that regulate the cell cycle downstream of the pre-BCR in control and DCKO late pre-B cells.

Here we demonstrate the transcription factors induced downstream of the pre-BCR that drive quiescence and VJ recombination in late pre-B cells are activated in the DCKO late pre-B cells and that these cells express the recombination machinery and undergo germline transcription of the Igκ locus. (A) Abundance of mRNAs in control (n=3) and DCKO (n=2) late pre-B cells measured by RNAseq. Samples were normalized according to the library size and compared using a negative binomial test with a Benjamini-Hochberg correction for multiple testing using DESeq. Adjusted p-values are shown. (B) Non-coding Igκ transcription upstream of the Igκ J segments measured by RNAseq in control (n=3) and DCKO (n=2) late pre-B cells expressed as reads per million. (C-F) Flow cytometric analysis of IRF4 (C), IRF8 (D), Ikaros (E) and Aiolos (F) expression in control (n=6 or 7) and DCKO (n=6 or 7) late pre-B cells. Representative histograms and summary data are shown. Median fluorescence intensities (MFIs) were normalized to the isotype control by subtracting the isotype MFI from the specific antibody MFI. Samples were compared by Student's t-tests. Symbols indicate biological replicates, bars represent means.

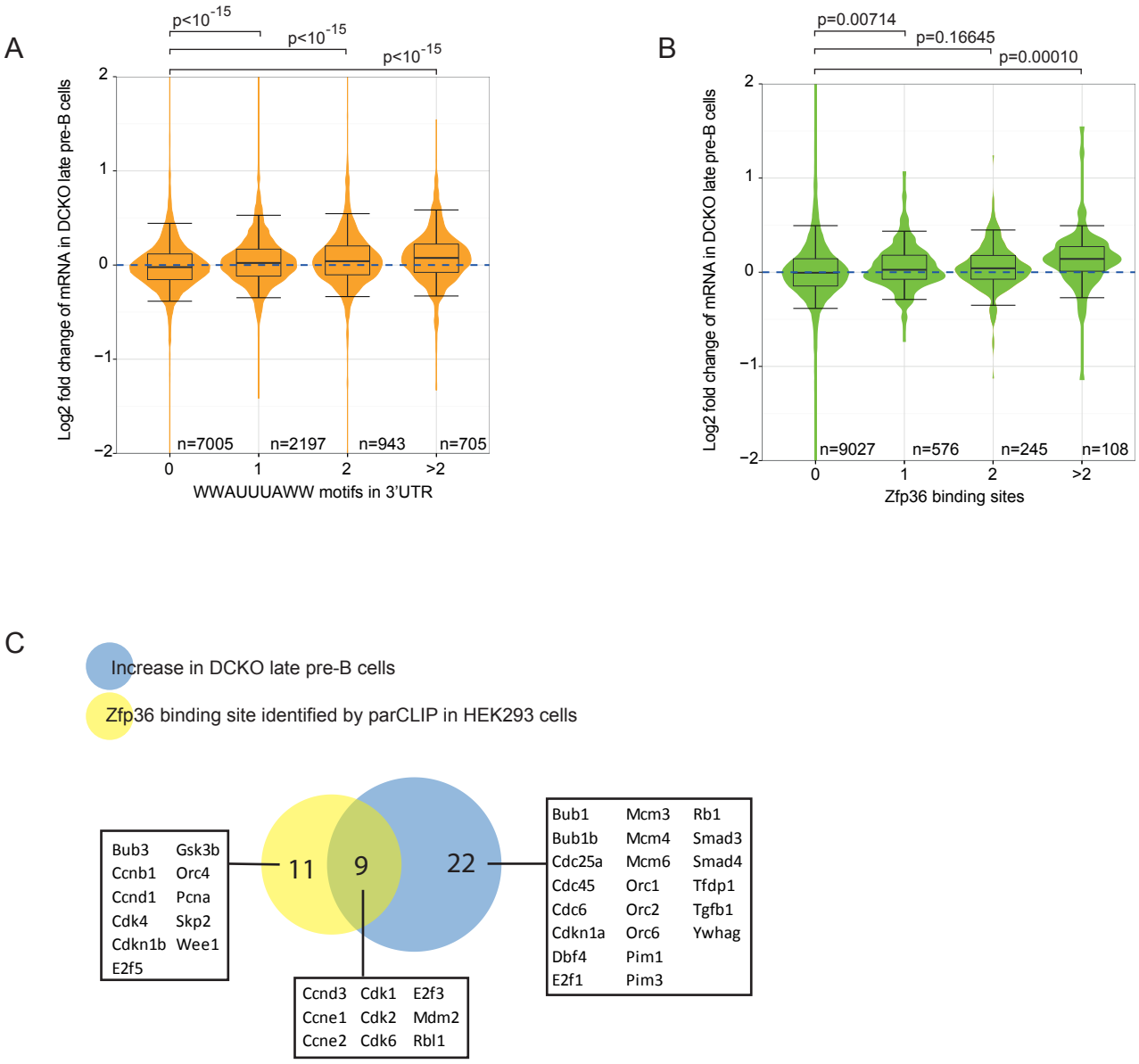

Fig. S8: Analysis of RNAseq data to assess the differences in expression of ARE and Zfp36 binding site-containing transcripts.
(A, B) Moderated log2 fold change in the abundance of mRNAs in DCKO compared to control late pre-B cells in mRNAs grouped by the number of AREs, defined as WWAUUUAWW (where W is A or U), in their 3'UTRs (A), or by the number of Zfp36 binding sites in the 3'UTR of their human homologue determined from published PAR-CLIP data (*15*) (B). n indicates the number of genes in each group. Boxes show median and interquartile range, whiskers indicate the 5th and 95th percentiles. Groups of mRNAs were compared by an ANOVA with Tukey's post-test. (C) Venn diagram of cell cycle mRNAs indicating overlap between mRNAs whose human homologues were identified as Zfp36 targets by PAR-CLIP, mRNAs with WWAUUUAWW motifs in their 3'UTRs, and mRNAs significantly increased in the DCKO late pre-B cells compared to control late pre-B cells as determined by a negative binomial test with a Benjamini-Hochberg correction for multiple testing in DESeq.

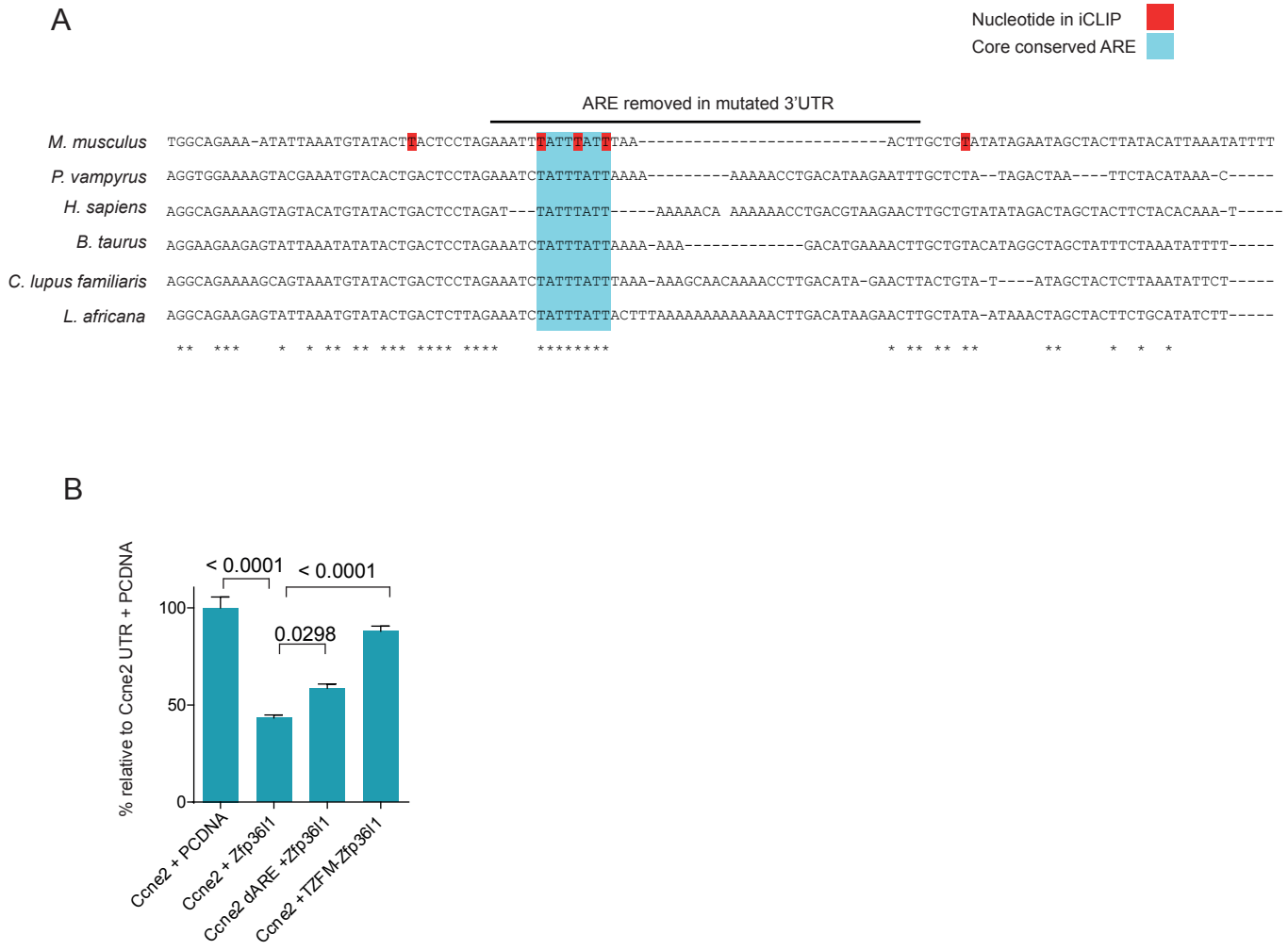

Fig. S9: An ARE identified in the *Ccne2* 3'UTR is responsive to ZFP36L1
(A) Section of the Ccne2 3'UTR showing alignments between *H. sapiens, M. musculus, L. Africana, P. vampyrus, C. lupus familaris* and *B. Taurus* sequences. Nucleotides identified by ZFP36L1 iCLIP and the core conserved ARE in the region are shown as well as the section removed in dARE mutant used for luciferase assays. (B) Ratio of firefly to renilla luciferase signal in lysates from HELA cells transfected with constructs with the full Ccne2 3'UTR or Ccne2 3'UTR with the ARE shown in (A) deleted, co-transfected with either an empty PCDNA plasmid, or PCDNA plasmid expressing wild-type ZFP36L1 or ZFP36L1 with mutations on both the RNA-binding zinc fingers (TZFM). Ratios were normalized to an empty luciferase construct and expressed as a percentage of the signal obtained with the Ccne2 UTR co-transfected with empty PCDNA.

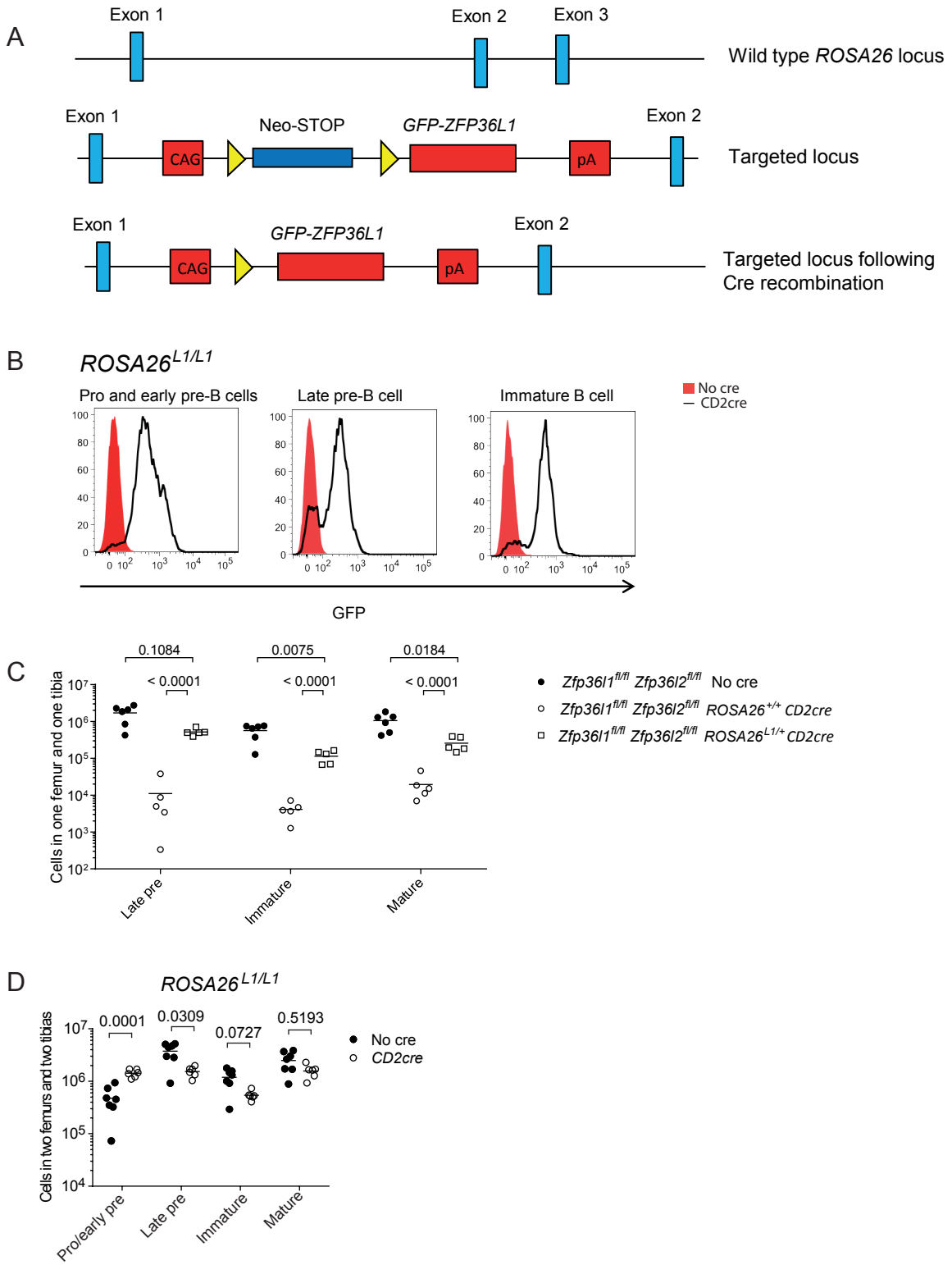

Fig. S10: Generation of the *ROSA26^{L1}* transgene.
(A) Targeting strategy of *ROSA26^{L1}* allele. (B) Representative histograms showing flow cytometric analysis of GFP expression in B cell developmental subsets in *ROSA26^{L1}* and *ROSA26$^{L1/L1}$ CD2cre* bone marrow. Data are representative of six mice of each genotype. (C) Flow cytometric quantification of B cell developmental subsets in *Zfp36l1$^{fl/fl}$ Zfp36l2$^{fl/fl}$* (n=6); *Zfp36l1$^{fl/fl}$ Zfp36l2$^{fl/fl}$ ROSA26$^{+/+}$ CD2cre* (n=5); and *Zfp36l1$^{fl/fl}$ Zfp36l2$^{fl/fl}$ ROSA26$^{L1/+}$ CD2cre* (n=5) bone marrow demonstrating that the *ROSA26^{L1}* transgene can functionally complement loss of *Zfp36l1* and *Zfp36l2* in B cell development. Data are representative of a single experiment. Symbols indicate biological replicates, and bars represent geometric means, populations were compared by an ANOVA with Tukey's post test. (D) Flow cytometric quantification of B cell developmental subsets in *ROSA26$^{L1/L1}$* (n=7) and *ROSA26$^{L1/L1}$ CD2cre* (n=6) bone marrow demonstrating a slight reduction in late pre-B cells, but recovery of cellularity by the mature B cell stage in *ROSA26$^{L1/L1}$ CD2cre* mice. Data are representative of two experiments. Symbols indicate biological replicates, and bars represent geometric means, populations were compared by an ANOVA with Sidak's post test.

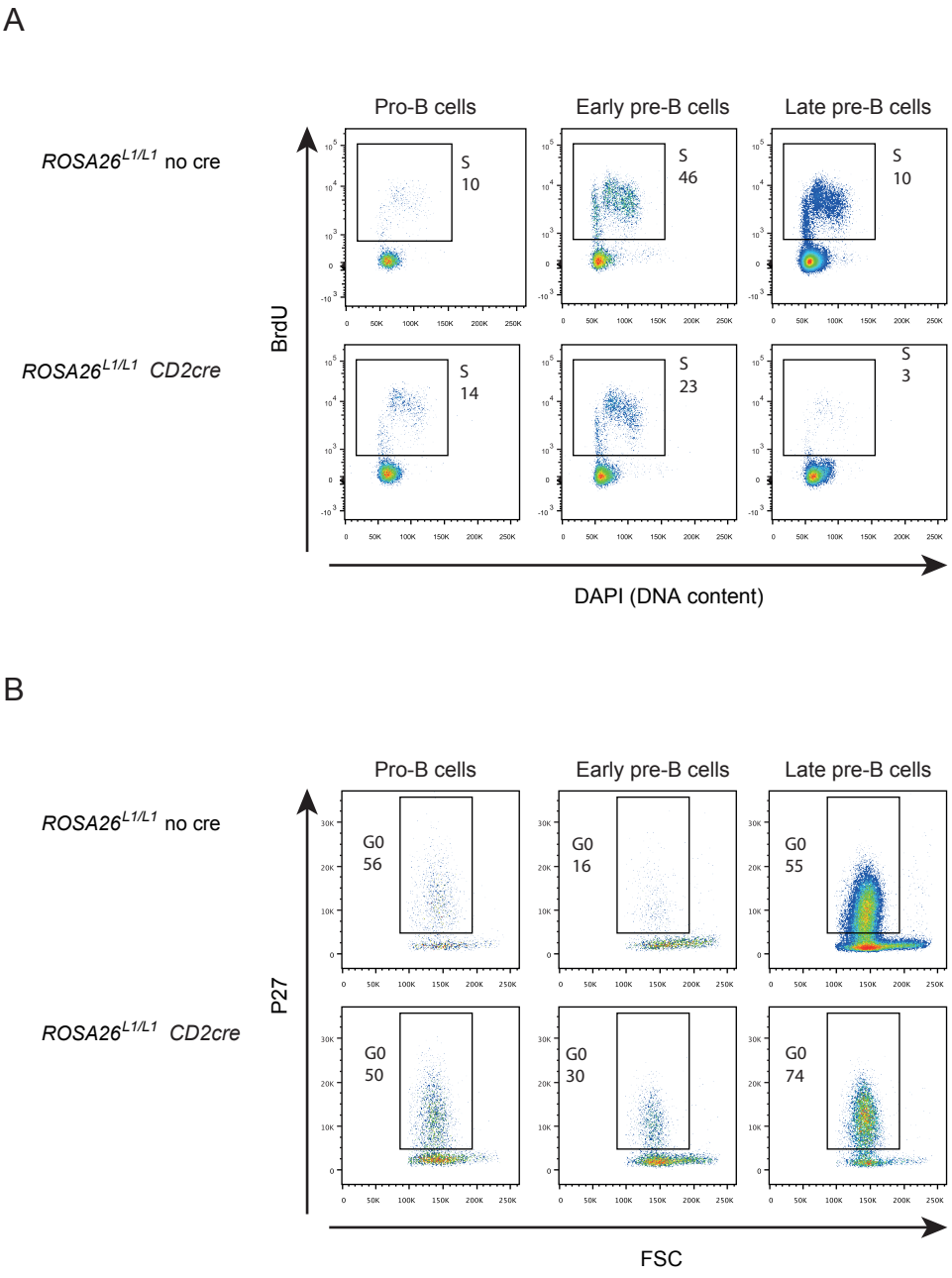

Fig. S11: Cell cycle analysis in *ROSA26$^{L1/L1}$ CD2cre* pro and pre-B cells.
(A) Representative dot plots from intracellular flow cytometry measuring BrdU incorporation following 2.5 hours labelling *in vivo* in *ROSA26$^{L1/L1}$* and *ROSA26$^{L1/L1}$ CD2cre* pro and pre-B cells. (B) Representative dot plots from intracellular flow cytometry measuring p27 in *ROSA26$^{L1/L1}$* and *ROSA26$^{L1/L1}$ CD2cre* pro and pre-B cells. Numbers on dot plots indicate the percentage of plotted cells in the gates.

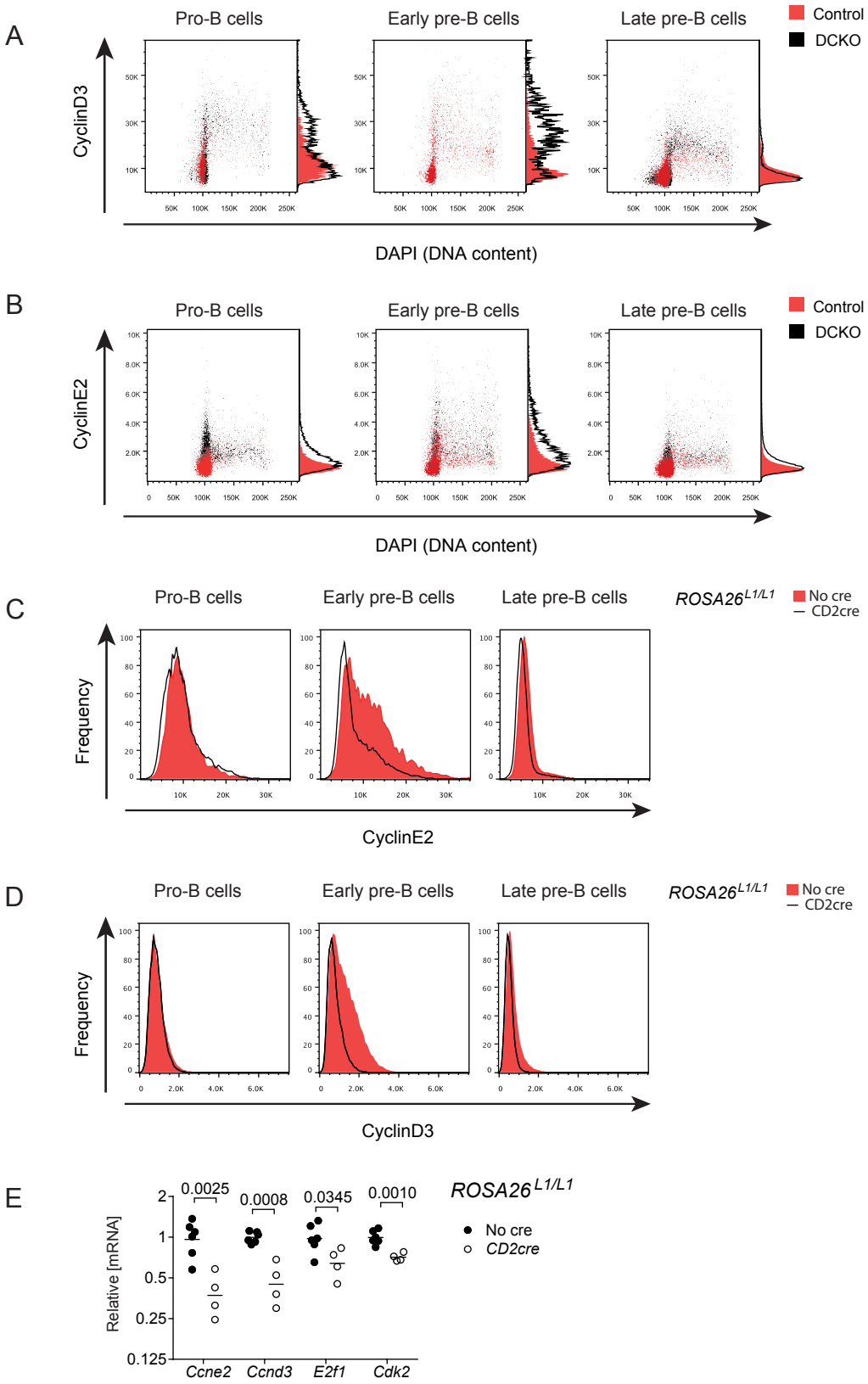

Fig. S12: Expression of cyclinD3 and cyclinE2 in DCKO and ROSA26$^{L1/L1}$ mice
(A, B) Representative flow cytometry dot plots and histograms showing cyclinE2 (A) and cyclinD3 (B) expression assayed by flow cytometry in control and DCKO pro- and pre-B cells. (C, D) Representative flow cytometry histograms showing cyclinE2 (C) and cyclinD3 (D) expression in *ROSA26*$^{L1/L1}$ and *ROSA26*$^{L1/L1}$ *CD2cre* pro and pre-B cells. (E) RT-qPCR measurements of the abundance of mRNAs proposed to be targets of ZFP36 family RBPs, in cDNA from sorted *ROSA26*$^{L1/L1}$ (n=6) and *ROSA26*$^{L1/L1}$ *CD2cre* (n=4) late pre-B cells. Measurements were normalized to *Tbp, Sdha, B2m* and *Ubc*. Bars represent geometric means. Data are representative of two independent experiments. *ROSA26*$^{L1/L1}$ and *ROSA26*$^{L1/L1}$ *CD2cre* data were compared using student's t-tests with a Holm-Sidak correction for multiple testing.

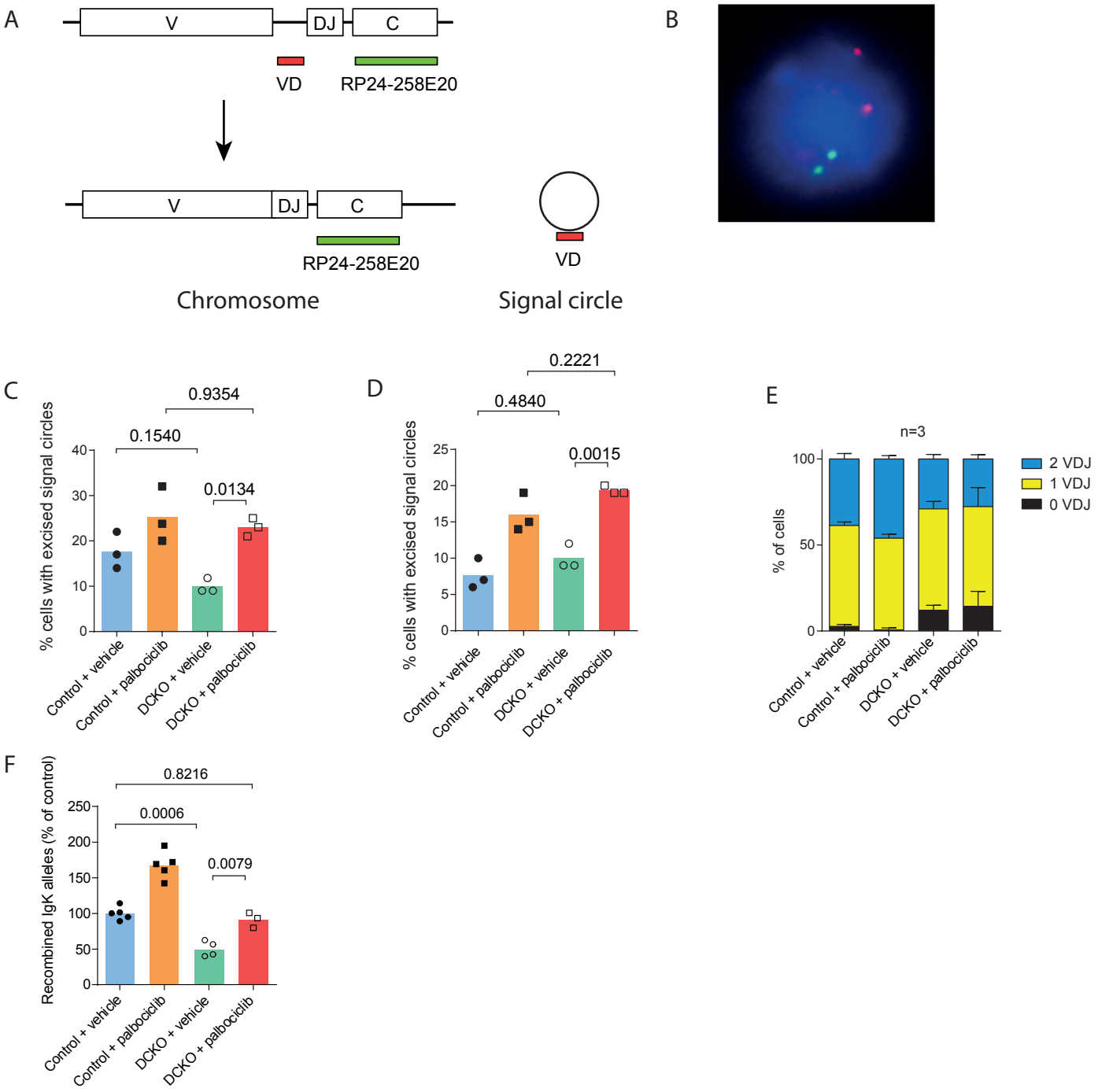

Fig. S13: Inhibition of CDK4 and CDK6 with palbociclib restores VDJ recombination in DCKO pro- and pre-B cells

(A) Diagram describing detection of recombined IgH loci and excised signal joints by DNA FISH. (B) Representative FISH image showing a cell containing two excision circles and two V to DJ recombined IgH alleles. (C) Percentage of pro/early pre-B cells containing excision circles from control and DCKO following treatment with vehicle control or 150mg/kg palbociclib daily for two days. Data are from a single experiment, n=3 for each group. (D) Percentage of late pre-B cells containing excision circles from control and DCKO following treatment with vehicle control or 150mg/kg palbociclib daily for two days. Data are from a single experiment, n=3 for each group. (E) Quantification of late pre-B cells with zero, one, or two V to DJ recombined IgH alleles by DNA FISH in control and DCKO mice following treatment with vehicle control or 150mg/kg palbociclib daily for two days. Data are from a single experiment, n=3 for each group, bars represent mean values, error bars indicate the standard deviation. (F) Abundance of recombined Igκ alleles, measured by qPCR, in the late pre-B cells of control and DCKO mice treated with vehicle control or 150mg/kg palbociclib daily for four days. Data are from a single experiment. Individual symbols, where shown, represent biological replicates and bars represent mean values. Control and DCKO samples were compared using an ANOVA with Tukey's post test.